www.nature.com/cr
www.cell-research.com

ARTICLE

Lin28a maintains a subset of adult muscle stem cells in an embryonic-like state

Peng Wang[1,2,3,10], Xupeng Liu[1,2,3,10], Ziyue Yao[1,2,3], Yu Chen[1,2,3], Lanfang Luo[1,2,3], Kun Liang[1,2,3], Jun-Hao Elwin Tan[4,5,6,7], Min-Wen Jason Chua[4,5,6,7], Yan-Jiang Benjamin Chua[4,5,6,7], Shilin Ma[1,2,3], Liping Zhang[1,2,3], Wenwu Ma[1,2,3], Shuqing Liu[1,2,3], Wenhua Cao[1,2,3], Luyao Guo[1,2,3], Lu Guang[1,2,3], Yuefan Wang[1,2,3], He Zhao[1,2,3], Na Ai[3,8], Yun Li[3,8], Chunwei Li[9], Ruiqi Rachel Wang[1,2], Bin Tean Teh[6,7], Lan Jiang[8], Kang Yu[9] and Ng Shyh-Chang[1,2,3]✉

During homeostasis and after injury, adult muscle stem cells (MuSCs) activate to mediate muscle regeneration. However, much remains unclear regarding the heterogeneous capacity of MuSCs for self-renewal and regeneration. Here, we show that Lin28a is expressed in embryonic limb bud muscle progenitors, and that a rare reserve subset of Lin28a$^+$Pax7$^-$ skeletal MuSCs can respond to injury at adult stage by replenishing the Pax7$^+$ MuSC pool to drive muscle regeneration. Compared with adult Pax7$^+$ MuSCs, Lin28a$^+$ MuSCs displayed enhanced myogenic potency in vitro and in vivo upon transplantation. The epigenome of adult Lin28a$^+$ MuSCs showed resemblance to embryonic muscle progenitors. In addition, RNA-sequencing revealed that Lin28a$^+$ MuSCs co-expressed higher levels of certain embryonic limb bud transcription factors, telomerase components and the p53 inhibitor Mdm4, and lower levels of myogenic differentiation markers compared to adult Pax7$^+$ MuSCs, resulting in enhanced self-renewal and stress-response signatures. Functionally, conditional ablation and induction of Lin28a$^+$ MuSCs in adult mice revealed that these cells are necessary and sufficient for efficient muscle regeneration. Together, our findings connect the embryonic factor Lin28a to adult stem cell self-renewal and juvenile regeneration.

Cell Research (2023) 33:712–726; https://doi.org/10.1038/s41422-023-00818-y

INTRODUCTION

Mammalian skeletal muscles possess strong regenerative capacities that decline with development and age. Skeletal muscle satellite cells, which undergo self-renewal and are necessary for adult muscle regeneration,[1] are a group of sublaminar muscle stem cells (MuSCs) embedded between the muscle fibrillar membrane and basal lamina. In injured muscles, MuSCs are activated and begin to proliferate as committed myogenic progenitor cells.[2] These cells fuse with existing myofibers, or form de novo myofibers, to achieve localized muscle regeneration.[3] It is well-known that embryonic myogenesis which lays down the entire body's musculature, is stronger than the adult myogenesis that occurs during localized regeneration after injury. However, little is known about the molecular mechanisms that underlie this phenomenon.

There are in fact multiple waves of myogenesis from different origins during mammalian development, which might give rise to different MuSC populations in adulthood.[4] While it is known that some sublaminar satellite cells are MuSCs, not every MuSC is a satellite cell. Pax7$^+$ satellite cells are the major source of adult MuSCs, while the presence and functions of other muscle-resident stem/progenitor populations remain less clear, including Pax3$^+$ MuSCs and Peg3$^+$ interstitial progenitor cells. On the other hand, there are clearly the non-myogenic Pdgfra$^+$ fibro-adipogenic progenitors (FAPs).[5–7] For instance, Pax3$^+$ MuSCs are thought to exist not just in the sublaminar niche, but also in the interstitium of the limb, diaphragm and various other muscles.[5] Mice with Pax7$^+$ satellite cell ablation still showed normal muscles.[8,9] Thus, there is possibly some heterogeneity among MuSCs, and not all MuSCs derive from sublaminar Pax7$^+$ satellite cells alone.

It is also not clear if all Pax7$^+$ MuSCs are equivalent. Previous studies showed that, curiously, there exists a population of Myf5$^-$Pax7$^+$ MuSCs that are less differentiated and more regenerative than Myf5$^+$Pax7$^+$ MuSCs.[10] Another mystery in muscle regeneration is the extraordinary variability in muscle aging and atrophy amongst human elderly, despite similarly large numbers of Pax7$^+$ MuSCs.[11] It is plausible that the most regenerative MuSCs that determine muscle aging, are actually hidden within a subtype of MuSCs, which are known to possess diverse developmental origins and thus developmental timings and epigenetic ages. In the hematopoietic system, it is the Flk2$^-$ long-term HSCs hidden within the Flk2$^+$ short-term HSCs that really determine hematopoietic aging.[12]

[1]Institute of Zoology, Chinese Academy of Sciences, Beijing, China. [2]Beijing Institute for Stem Cell and Regenerative Medicine, Institute for Stem Cell and Regeneration, Chinese Academy of Sciences, Beijing, China. [3]University of Chinese Academy of Sciences, Beijing, China. [4]NUS Graduate School for Integrative Sciences and Engineering, National University of Singapore, Singapore, Singapore. [5]Institute of Molecular and Cell Biology, Genome Institute of Singapore, Agency for Science Technology and Research, Singapore, Singapore. [6]Laboratory of Cancer Therapeutics, Program in Cancer and Stem Cell Biology, Duke-National University of Singapore Medical School, Singapore, Singapore. [7]Laboratory of Cancer Epigenome, Division of Medical Science, National Cancer Centre Singapore, Singapore, Singapore. [8]CAS Key Laboratory of Genome Sciences and Information, Beijing Institute of Genomics, Chinese Academy of Sciences, Beijing, China. [9]Department of Clinical Nutrition, Peking Union Medical College Hospital, Chinese Academy of Medical Sciences & Peking Union Medical College, Beijing, China. [10]These authors contributed equally: Peng Wang, Xupeng Liu. ✉email: huangsq@ioz.ac.cn

Received: 21 September 2022 Accepted: 23 April 2023
Published online: 15 May 2023

In nematodes and mammals, the *Lin28* gene is highly expressed during early embryogenesis, but gradually diminishes by adulthood. *Lin28* is one of the first genes discovered to regulate developmental timing in nematodes, and this regulation is related to the self-renewal of stem cells.[13–15] The function of Lin28 can be explained by its role as an RNA-binding protein, which acts on the *let-7* microRNA and many other mRNAs.[16–20] Loss of *Lin28* accelerates differentiation during embryogenesis, while gain of *Lin28* promotes self-renewal during embryogenesis.[21] Mammalian studies have revealed that ectopic *Lin28* can promote wound repair,[22] but the endogenous roles of *Lin28* in bona fide adult stem cell-based regeneration remain unclear. Endogenous *Lin28a* was reported to be one of the genes expressed during muscle regeneration,[23] but it is unclear whether *Lin28a* plays a functional role in MuSC-based regeneration. This is in part because no lineage-tracing studies have been performed with *Lin28a*, a challenging problem for promoter-driven Cre mice, given that *Lin28a* mRNA expression is heavily regulated post-transcriptionally.[24]

Here we tagged Lin28a protein with a "self-cleaving" CreER recombinase to trace Lin28a$^+$ cell lineages in adult muscles. We found a previously unknown and rare subset of Lin28a$^+$Pax7$^-$ MuSCs that can replenish the Pax7$^+$ MuSC pool, regenerate all subtypes of muscle fibers in adult muscle, and possess epigenomic characteristics of embryonic limb muscle progenitors. As a result of *Lin28a*-regulated gene expression, Lin28a$^+$ MuSCs manifest higher stress-responsiveness and self-renewal capacity, with increased myogenicity in vitro and in vivo. Conditional ablation of Lin28a$^+$ MuSCs compromised, while injury-induced activation of Lin28a$^+$ MuSCs promoted adult muscle regeneration in vivo, showing that juvenilized Lin28a$^+$ MuSCs are necessary and sufficient to mediate efficient adult muscle regeneration.

RESULTS

Lin28a$^+$ cells exist in embryonic limbs and contribute to adult MuSCs

To observe whether the post-transcriptionally regulated *Lin28a* is expressed in any particular subset of muscle cells, we tagged endogenous Lin28a protein with a "self-cleaving" T2A-CreER at its C-terminus using homologous recombination. This "self-cleaving" design ensured that the *Lin28a-T2A-CreER* mRNA was regulated post-transcriptionally in the same way as endogenous *Lin28a* mRNA, and ensured that CreER protein was expressed if and only if endogenous Lin28a protein was expressed, without disrupting endogenous Lin28a protein function. We constructed *Lin28a-T2A-CreER* transgenic mice (Supplementary information, Fig. S1a, b), and bred them with *Rosa26-loxp-stop-loxp (LSL)-tdTomato* (tdTO) reporter mice to trace the fate(s) of Lin28a$^+$ cells after muscle injury. After 1 day of lineage tracing in embryonic day (E) 11.5 embryos, we found that embryonic Lin28a$^+$ limb muscle progenitor cells gave rise to myofibers during embryonic limb development at E12.5 (Supplementary information, Fig. S1c). We traced another batch of 6-month-old adult mice, and found that after 20 days of tracing (Fig. 1a), tibialis anterior (TA) muscles of uninjured mice still had a small number of adult Lin28a-tdTO$^+$ mononucleated cells adjacent to some muscle fibers (Fig. 1b), as well as a small number of tdTO$^+$ muscle fibers, suggesting that primitive adult Lin28a$^+$ stem cells existed and could fuse with ~10% of the adult TA muscle fibers during normal muscle homeostasis (Fig. 1b). Upon injury, the numbers of Lin28a-tdTO$^+$ cells and tdTO$^+$ muscle fibers were both significantly increased (Fig. 1b, c), suggesting that injury stimulated Lin28a$^+$ stem cell proliferation and increased fusion with existing myofibers by over 3-fold (Fig. 1c). In a muscle group with slower turnover (soleus (SOL) muscles),[25] the number of Lin28a-tdTO$^+$ myofibers was still significantly increased after injury (Fig. 1b, c). These rare Lin28a-tdTO$^+$ adult skeletal muscle cells were isolated by fluorescence-activated cell sorting (FACS), and their Lin28a protein expression was confirmed by low-protein-input capillary-based immunoassays (Fig. 1d).

When Lin28a-tdTO$^+$ skeletal muscle cells were cultured in vitro, the expression of both Lin28a protein and the CreER protein was extinguished simultaneously, indicating that the turnover of "cleaved" T2A-CreER was just as rapid as Lin28a, which enabled high-fidelity labeling of Lin28a$^+$ cells (Supplementary information, Fig. S2a). To ensure that the expression of endogenous Lin28a was not significantly interfered by the T2A-CreER tag, we examined total Lin28a protein expression in heterozygous *Lin28a-T2A-CreER* mice, and found no significant differences between wild-type and *Lin28a-T2A-CreER* mice (Supplementary information, Fig. S2b). Thus, our novel lineage-tracing system can accurately identify bona fide Lin28a$^+$ cells.

To clarify the identity of Lin28a$^+$ stem cells, we quantified Lin28a-tdTO$^+$ cells that expressed Pax7 or Pax3, before and after injury. Pax7 is generally regarded as the definitive marker of sublaminar satellite stem cells that proliferate and develop into skeletal muscles during postnatal growth;[26,27] however, reports have also shown that some MuSCs express Pax3 as well.[5,28,29] Immunofluorescence results showed that ~70% of the rare Lin28a-tdTO$^+$ cells were located in the sublaminar region just like Pax7$^+$ satellite stem cells, while ~30% were located in the interstitium (Fig. 1e). Interestingly, only a small fraction of the rare Lin28a-tdTO$^+$ cells co-expressed Pax7 or Pax3 before injury, and the majority were Pax7$^-$ and Pax3$^-$ (Fig. 1f–h and Supplementary information, Fig. S1d). These results were corroborated by the rare co-expression of Pax3 and Pax7 in Lin28a-tdTO$^+$ cells (Supplementary information, Fig. S2c). After injury, we observed a decrease in Lin28a-tdTO$^+$Pax7$^-$ cells (~20%) and a significant increase in Lin28a-tdTO$^+$Pax7$^+$ cells (~24%) (Fig. 1h). The total percentage of Pax7$^+$ satellite cells that were labeled by tdTO fluorescence rose from ~1% before injury to ~18% after injury (Fig. 1i). These results indicated that the rare Lin28a$^+$ cells can serve as a reserve population that replenishes some of the adult Pax7$^+$ MuSC compartment during adult muscle regeneration. In comparison, the proportions of Pax3$^+$ and Pax3$^-$ cells in the Lin28a-tdTO$^+$ pool remained largely unchanged after injury due to self-renewal (Fig. 1h), although the small portion of Pax3$^+$ MuSCs that were Lin28a-tdTO$^+$ rose slightly after injury (Fig. 1j). These results suggest that Lin28a-tdTO$^+$ progeny are derived from Lin28a$^+$Pax3/7$^-$ MuSCs after injury. Alternatively, if Lin28a-tdTO$^+$ progeny were mainly derived from Lin28a$^-$Pax3/7$^+$ MuSCs, then Lin28a-tdTO$^-$Pax3/7$^+$ cells should increase after injury as expected, but Lin28a$^+$Pax3/7$^-$ cells should increase even more, because this subset should be amplifying the initial expansion of Pax3/7$^+$ cells as downstream progeny for the first time in adulthood.

However, we observed that Lin28a$^+$Pax3/7$^-$ did not increase after muscle injury. This quantitative result contradicts expectations from the alternative hypothesis, and directly supports our conclusion that Lin28a$^+$Pax3/7$^-$ stem cells are the main source of Lin28a-tdTO$^+$ progeny.

Taken together, our low-protein-input capillary-based immunoassays and tdTO lineage tracing results suggest that there exist a rare population of reserve adult MuSCs expressing Lin28a protein but not Pax7 or Pax3 before injury. During MuSC expansion after injury, a significant proportion of these Lin28a$^+$-Pax3$^-$Pax7$^-$ MuSCs become lineage-committed to replenish some of the Pax7$^+$ satellite cells and other MuSCs, suggesting a role for reserve Lin28a$^+$ MuSCs in the self-renewal of adult MuSC pools and skeletal muscle regeneration in general.

Rare Lin28a$^+$ stem cells contribute to all myofibers during regeneration

To test the regenerative capacity of Lin28a$^+$ MuSCs vs adult Pax7$^+$ MuSCs in vivo, we isolated equal numbers of Lin28a-tdTO$^+$ MuSCs

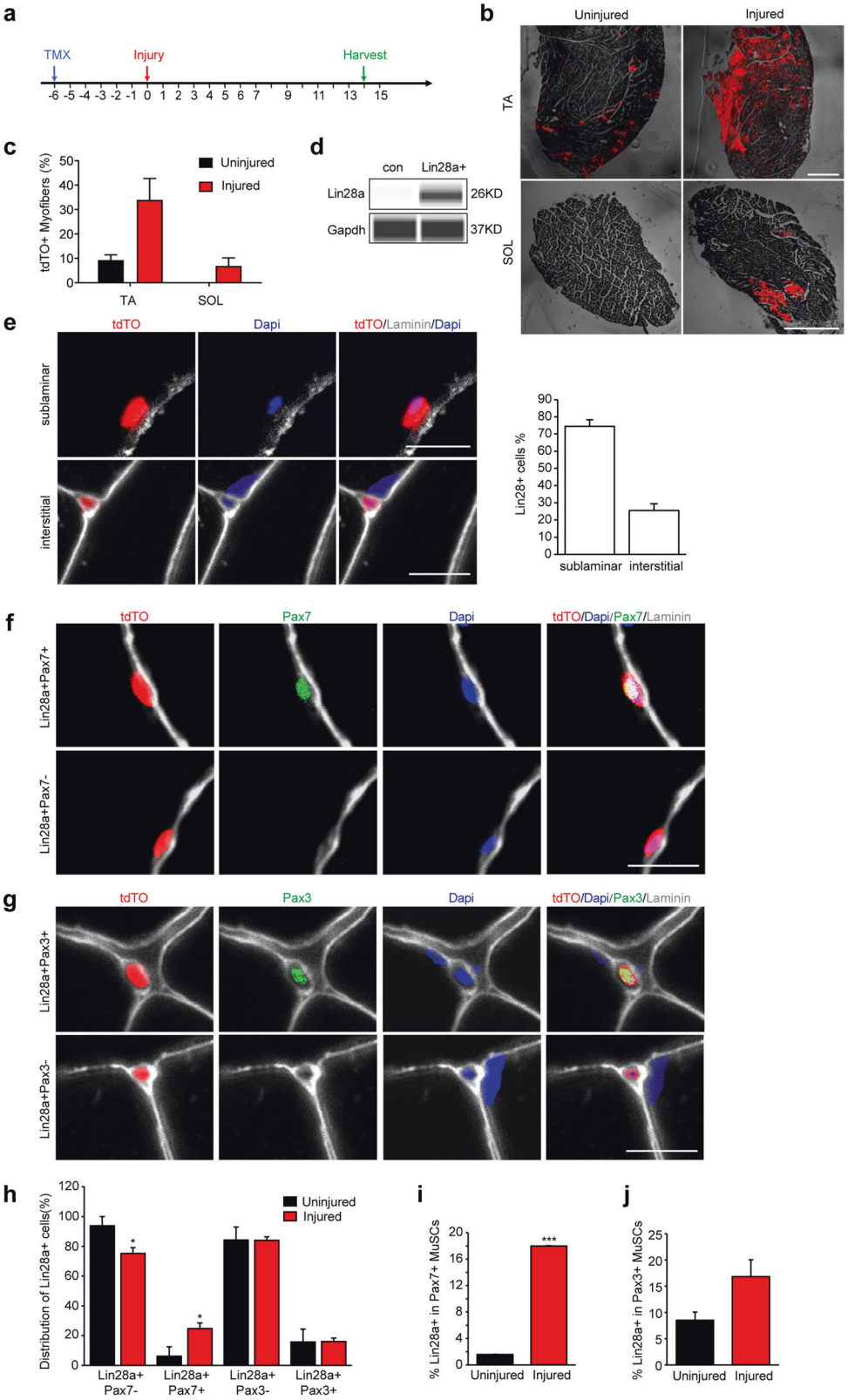

and adult Pax7$^+$ MuSCs by FACS, and transplanted them orthotopically into the cryoinjured TA muscles of immunodeficient NSG mice. Tracing of tdTO$^+$ myofibers showed that Lin28a$^+$ MuSCs were superior to conventional Pax7$^+$ MuSCs in engraftment rate, fusion efficiency, and myogenic potency during regeneration in vivo (Fig. 2a, b).

Upon differentiation, skeletal myofibers show diversity in metabolic and physical functions, with each muscle group containing a mixture of different types of muscle fiber fates, e.g., type I, IIa, IIx, and IIb myofibers. These myofibers can be roughly classified as slow-twitch (I) and fast-twitch (IIa, IIx, IIb), or oxidative (I, IIa) and glycolytic (IIx, IIb).[30] Given the difference in Lin28a-tdTO

Fig. 1 Lin28a$^+$ stem cells contribute to satellite cells and myofibers during regeneration. a Schedule of tamoxifen (TMX) treatment. *Lin28a-T2A-CreER;LSL-tdTO* mice were injected with TMX, 6 days before cryoinjury, daily for the first 1 week after injury, every other day from the 7th day, and harvested on the 14th day after injury. **b** TA and SOL muscles of *Lin28a-T2A-CreER;LSL-tdTO* mice were damaged by cryoinjury and harvested on day 14 post injury. Contralateral TA or SOL muscle was used as the control. Scale bars, 600 μm. **c** Quantification of the number of tdTO$^+$ muscle fibers per 100 muscle fibers in the TA and SOL muscles of *Lin28a-T2A-CreER;LSL-tdTO* mice on day 14 post injury and without injury. Quantification was performed on the images in **b**. For each muscle section, at least 3 whole sections were quantified and averaged. **d** Low-protein-input capillary-based immunoassays for Lin28a protein expression in Lin28a-tdTO$^+$ and conventional (con) Pax7$^+$ MuSCs. Gapdh protein was used as the loading control. Unprocessed original capillary-based immunoassay results are shown in Supplementary information, Fig. S7. **e** Cryosections of the TA muscles of *Lin28a-T2A-CreER;LSL-tdTO* mice that were cryoinjured and harvested on day 14 post injury. Muscle sections were co-stained for laminin (white) and DAPI (blue). Scale bars, 10 μm. Right: quantification of the percentage of sublaminar and interstitial Lin28a$^+$ cells. For each muscle section, at least five different fields were quantified and averaged. **f** Cryosections of the TA muscle of *Lin28a-T2A-CreER;LSL-tdTO* mice at 14 days after cryoinjury. Muscle sections were co-stained for laminin (white), DAPI (blue) and Pax7 (green). Scale bar, 10 μm. **g** Cryosections of the TA muscle of *Lin28a-T2A-CreER;LSL-tdTO* mice at 14 days after cryoinjury. Muscle sections were co-stained for laminin (white), DAPI (blue) and Pax3 (green). Scale bar, 10 μm. **h** Quantification of the distribution of Pax3$^-$, Pax3$^+$, Pax7$^-$ and Pax7$^+$ cells in the Lin28a-tdTO$^+$ pool per field in the TA muscle of *Lin28a-T2A-CreER;LSL-tdTO* mice on day 14 post injury (red), relative to uninjured muscles (black). For each muscle section, at least five different fields were quantified and averaged. **i** Quantification of the percentage of Lin28a-tdTO$^+$ cells in Pax7$^+$ satellite cells per field in the TA muscle of *Lin28a-T2A-CreER;LSL-tdTO* mice on day 14 post injury (red), relative to uninjured muscles (black). For each muscle section, at least five different fields were quantified and averaged. **j** Quantification of the percentage of Lin28a-tdTO$^+$ cells in Pax3$^+$ MuSCs per field in the TA muscle of *Lin28a-T2A-CreER;LSL-tdTO* mice on day 14 post injury (red), relative to uninjured muscles (black). For each muscle section, at least five different fields were quantified and averaged. *$P < 0.05$, ***$P < 0.001$.

labeling efficiency in fast-twitch TA and slow-twitch SOL muscles, we sought to determine whether Lin28a-tdTO$^+$ MuSCs show myofiber specificity. Immunofluorescence staining of uninjured mouse muscle fibers showed that during the 20-day lineage tracing window, Lin28a-tdTO$^+$ MuSCs could contribute to type IIA, IIB, and IIX muscle fibers in TA muscles during normal homeostasis (Fig. 2c), but not the type I myofibers in SOL muscles (Fig. 2c, d). However, after injury, Lin28a-tdTO$^+$ MuSCs could contribute robustly to all types of muscle fibers in both slow-twitch SOL and fast-twitch TA muscles (Fig. 2d). These results suggest that Lin28a$^+$ MuSCs have the potential to contribute to all types of muscle fibers after proliferation and differentiation during skeletal muscle regeneration in vivo.

Lin28a$^+$ cells are VCAM1$^+$CD31$^+$Sca1$^+$ MuSCs

In order to further determine the properties of Lin28a-tdTO$^+$ cells, relative to conventional Pax7$^+$ MuSCs, we used flow cytometry to analyze these cell populations. We observed that Lin28a-tdTO$^+$ cells increased significantly only after muscle injury ($P < 0.001$) (Fig. 3a–c). To further characterize these tdTO$^+$ cells, we used different cell surface marker antibodies: CD31 (endothelial lineage), CD45 (hematopoietic lineage), Sca1 (mesodermal progenitor), VCAM1 (adult Pax7$^+$ MuSCs) to label these cells.[31] Flow cytometry analysis revealed that tdTO$^+$ cells were mostly CD45$^-$ (Fig. 3d) and VCAM1$^+$, similar to adult Pax7$^+$ MuSCs.[31]

However, the rare Lin28a-tdTO$^+$ MuSCs made up only a small subset of the total pool of VCAM1$^+$ cells (0.73%). Another key difference is that adult Pax7$^+$ MuSCs are CD31$^-$ and Sca1$^-$, whereas the majority of Lin28a$^+$ MuSCs were CD31$^+$ and Sca1$^+$ (Fig. 3d), suggesting again that they are reserve primitive cells originating from embryonic limb bud mesoderm.

To test the potency of adult Lin28a$^+$ cells, we attempted to differentiate freshly sorted Lin28a$^+$ cells into vascular endothelial cells, adipocytes or osteoblasts. The results showed that after Lin28a$^+$ cells were cultured in adipogenic, osteogenic, and endothelial cell media, respectively, most of the cells underwent senescence or apoptosis, and could not further differentiate, although a small fraction (~20%) did differentiate into osteoblasts in osteogenic medium (Supplementary information, Fig. S3a–d). In vivo immunofluorescence analysis for osteocalcin, a definitive marker of osteoblasts, showed that ~28% of the Lin28a$^+$ MuSCs expressed osteocalcin, suggesting their low osteogenic potential (Supplementary information, Fig. S3e). Nevertheless, adult Lin28a$^+$ cells did not show the tri-lineage potential of mesenchymal stem cells, and all the cells activated MyoD protein expression, suggesting that they strongly preserved the myogenic potential but only weakly preserved the osteogenic potential of embryonic limb bud mesoderm cells.

In order to further compare the myogenic potential of adult Lin28a$^+$Pax7$^-$ MuSCs (tdTO$^+$VCAM1$^+$CD31$^+$Sca1$^+$ cells) with Lin28a$^-$Pax7$^+$ MuSCs (tdTO$^-$VCAM1$^+$CD31$^-$Sca1$^-$ cells), Lin28a$^+$ cells were proliferated and differentiated in myogenic growth medium (GM) and differentiation medium (DM), respectively, and then immunofluorescence staining was performed. The results showed that upon culture in vitro, all the Lin28a$^+$Pax7$^-$ cells activated the muscle stem/progenitor cell markers Pax7 and MyoD when proliferating (Fig. 3e), and they could robustly form multinucleated myotubes expressing myosin heavy chain (MHC) proteins upon differentiation (Fig. 3f, g). To totally exclude the possibility of low-level contamination from conventional Pax7$^+$ MuSCs, we FACS-isolated single tdTO$^+$VCAM1$^+$CD31$^+$Sca1$^+$ cells, and tested them for differentiation in a single-cell clonogenic assay. All single-cell clones survived, proliferated, differentiated and formed multinucleated myotubes which could express MHC (Fig. 3h, i). Upon induced differentiation, the expression of many muscle stem/progenitor cell markers such as *Pax7*, *MyoD*, *Myf5* were downregulated as expected of MuSCs, while the expression of many myogenic differentiation-related genes such as muscle creatine kinase (*Ckm*) and the MHCs (*Myh1*, *Myh2* and *Myh4*) were upregulated significantly (Fig. 3j). These results indicate that Lin28a$^+$ MuSCs proliferate as skeletal muscle progenitors in vitro, and exhibit robust myogenic potency for fusion into multinucleated myotubes when induced to differentiate.

Lin28a$^+$Pax7$^-$ MuSCs show higher myogenicity than Lin28a$^-$Pax7$^+$ MuSCs

In order to compare the fusion efficiency of Lin28a$^+$ MuSCs with conventional Pax7$^+$ MuSCs, we cultured Lin28a$^+$Pax7$^-$ MuSCs, conventional Lin28a$^-$Pax7$^+$ MuSCs, and 1:1 mixed cells, and measured their fusion index after induction of differentiation. We observed that Lin28a$^+$Pax7$^-$ MuSC-derived myotubes were thicker in diameter and thus more hypertrophic, compared to conventional Lin28a$^-$Pax7$^+$ MuSC-derived myotubes (Fig. 4a, b; $P = 6.15 \times 10^{-7}$). Furthermore, our results showed that Lin28a$^+$-Pax7$^-$ MuSCs had a higher fusion index than conventional Lin28a$^-$Pax7$^+$ MuSCs, suggesting that Lin28a$^+$ MuSCs have higher myogenic potency than conventional Pax7$^+$ MuSCs both in vivo and in vitro (Figs. 2a and 4c).

To further compare the molecular differences between Lin28a$^+$ MuSCs and conventional Pax7$^+$ MuSCs in culture, we compared the myogenic factor expression of the two groups in vitro by quantitative RT-PCR (qRT-PCR) and Western blot analysis. We found that, compared with conventional Pax7$^+$ MuSCs, Lin28a$^+$ MuSCs expressed more Pax3 protein in GM (Fig. 4d). Upon exposure to cues for terminal differentiation, Lin28a$^+$ MuSC-

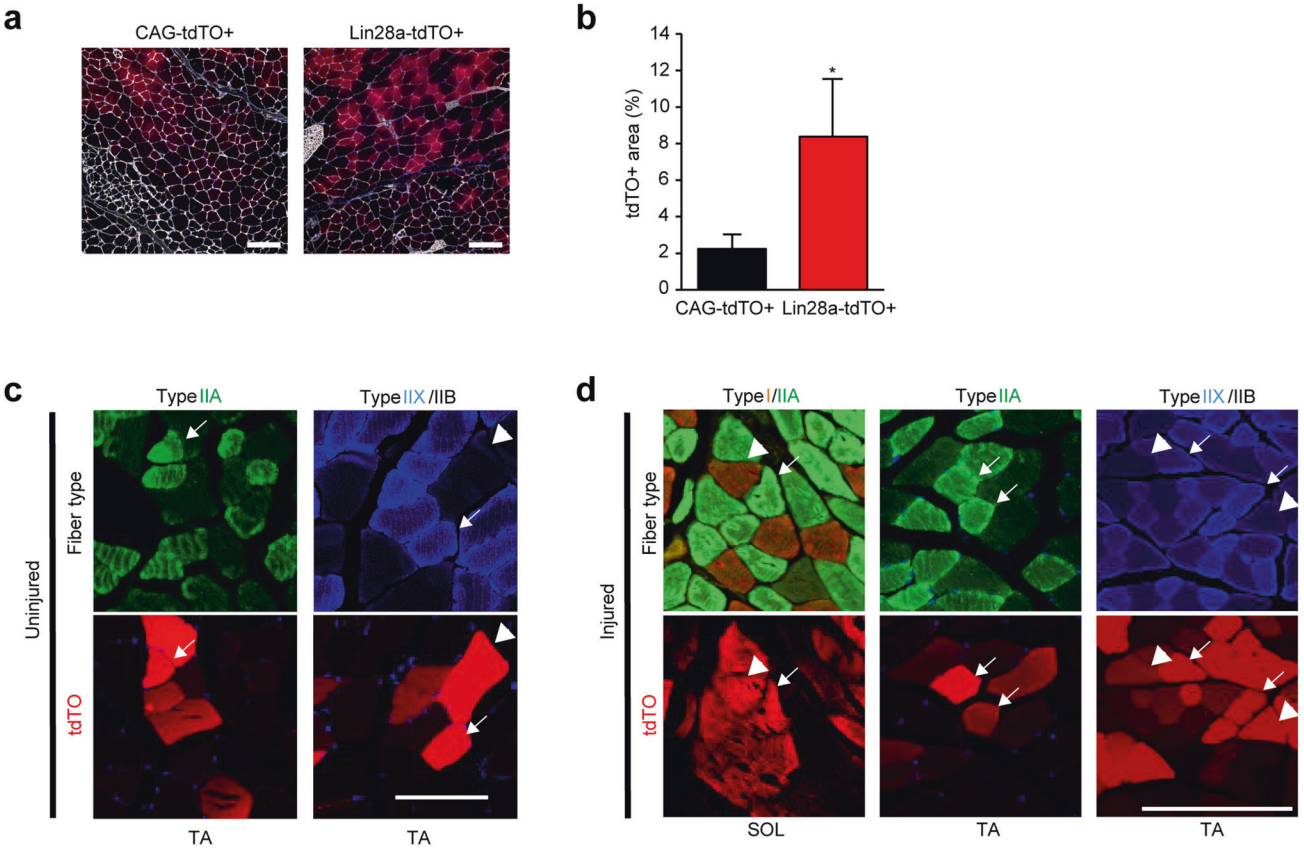

Fig. 2 Lin28a$^+$ stem cells contribute to myofibers during regeneration. a Cryosection and laminin immunofluorescence staining of TA muscles of NSG mice at 21 days after 1000 Lin28a-tdTO$^+$ MuSCs or Pax7$^+$ MuSCs (CAG-tdTO$^+$) were freshly sorted by FACS and transplanted orthotopically into cryoinjured TA muscles. Scale bars, 100 μm. **b** Proportion of tdTO$^+$ myofiber area in the cryoinjured TA region. Data are means ± SEM. $n = 3$ independent experiments. For each experiment, a total of 20 serial cryosections were counted and averaged. **c** Immunostaining of transverse sections of uninjured TA muscles obtained from *Lin28a-T2A-CreER;LSL-tdTO* mice at day 14 of lineage tracing, for type IIA (green), type IIX (blue) and type IIB (black) myofibers, compared to tdTO$^+$ fluorescence (arrowheads). Scale bar, 100 μm. **d** Immunostaining of transverse sections of injured SOL and TA muscles obtained from *Lin28a-T2A-CreER;LSL-tdTO* mice at day 14 of lineage tracing, for type I (red), type IIA (green), type IIX (blue) and type IIB (black) myofibers, compared to tdTO$^+$ fluorescence (arrowheads). Scale bar, 200 μm. *$P < 0.05$.

derived myotubes expressed more MHC protein and MyoG protein, than conventional Pax7$^+$ MuSC-derived myotubes (Fig. 4e). Quantification of mRNA expression reflected a similar pattern, where Lin28a$^+$ MuSCs expressed significantly higher levels of *Pax3* than conventional Pax7$^+$ MuSCs in GM (Fig. 4d). After induction of terminal differentiation, Lin28a$^+$ MuSC-derived myotubes expressed higher levels of *MyoG*, *Ckm*, *Myh1*, and *Myh4* than conventional Pax7$^+$ MuSC-derived myotubes (Fig. 4e). Notably, these differences in myogenic potential persisted although *Lin28a* expression was extinguished within 24 h of culture in vitro (Supplementary information, Fig. S4a, b). Taken together, these results indicate that Lin28a$^+$ MuSCs are distinct from conventional Pax7$^+$ MuSCs in their myogenic potency, at both the functional and molecular levels.

Epigenomic profiles show the similarity between Lin28a$^+$ MuSCs and embryonic muscle progenitors

Given these intrinsic differences in myogenic potency and the previous studies that suggested the presence of a DNA methylation epigenetic clock which reliably marks developmental timing from embryonic stem cells to adult somatic cells to senescent cells in mammals,[32,33] we were motivated to understand the epigenomic profile of Lin28a$^+$ MuSCs at the genome-wide level. We compared adult Lin28a$^+$ MuSCs to E12.5 embryonic muscle progenitors[34] and adult conventional Pax7$^+$ MuSCs ($n = 3$ mice each) through whole-genome bisulfite sequencing (WGBS; Supplementary information, Fig. S5a). Hierarchical clustering dendrograms indicated that adult Lin28a$^+$ MuSCs were more similar to embryonic muscle progenitors than expected (Fig. 5a). There were 5 clusters of differentially methylated regions in the dendrogram, instead of the 8 clusters expected by random chance, suggesting a more well-structured dendrogram than expected by chance (Fig. 5a). Clusters 1 and 4 indicated the expected similarities between the two adult MuSCs. Cluster 3, indicated the surprising similarities between adult Lin28a$^+$ MuSCs and embryonic muscle progenitors.

Clusters 2 and 5 indicated the epigenetic uniqueness of the Lin28a$^+$ MuSCs as a distinct subset of MuSCs. In particular, cluster 2 of silenced genes was enriched for muscle development- and epithelialization-related genes according to Gene Ontology (GO) analysis (Fig. 5b and Supplementary information, Fig. S5b), suggesting that Lin28a$^+$ MuSCs have silenced multiple genes for skeletal muscle differentiation and that, prior to cues for terminal differentiation, Lin28a$^+$ MuSCs are less differentiated than Pax7$^+$ MuSCs. Cluster 3 of silenced genes was enriched for adult muscle-associated calcium signaling for contractility, axon guidance signaling for neuromuscular junctions, phospholipase D signaling[35] and growth hormone signaling for hypertrophic growth, according to KEGG analysis (Fig. 5c and Supplementary information, Fig. S5c). These epigenomic results showed that adult Lin28a$^+$ MuSCs resembled embryonic muscle progenitors, where many adult muscle-associated genes were silenced. Cluster 5 of

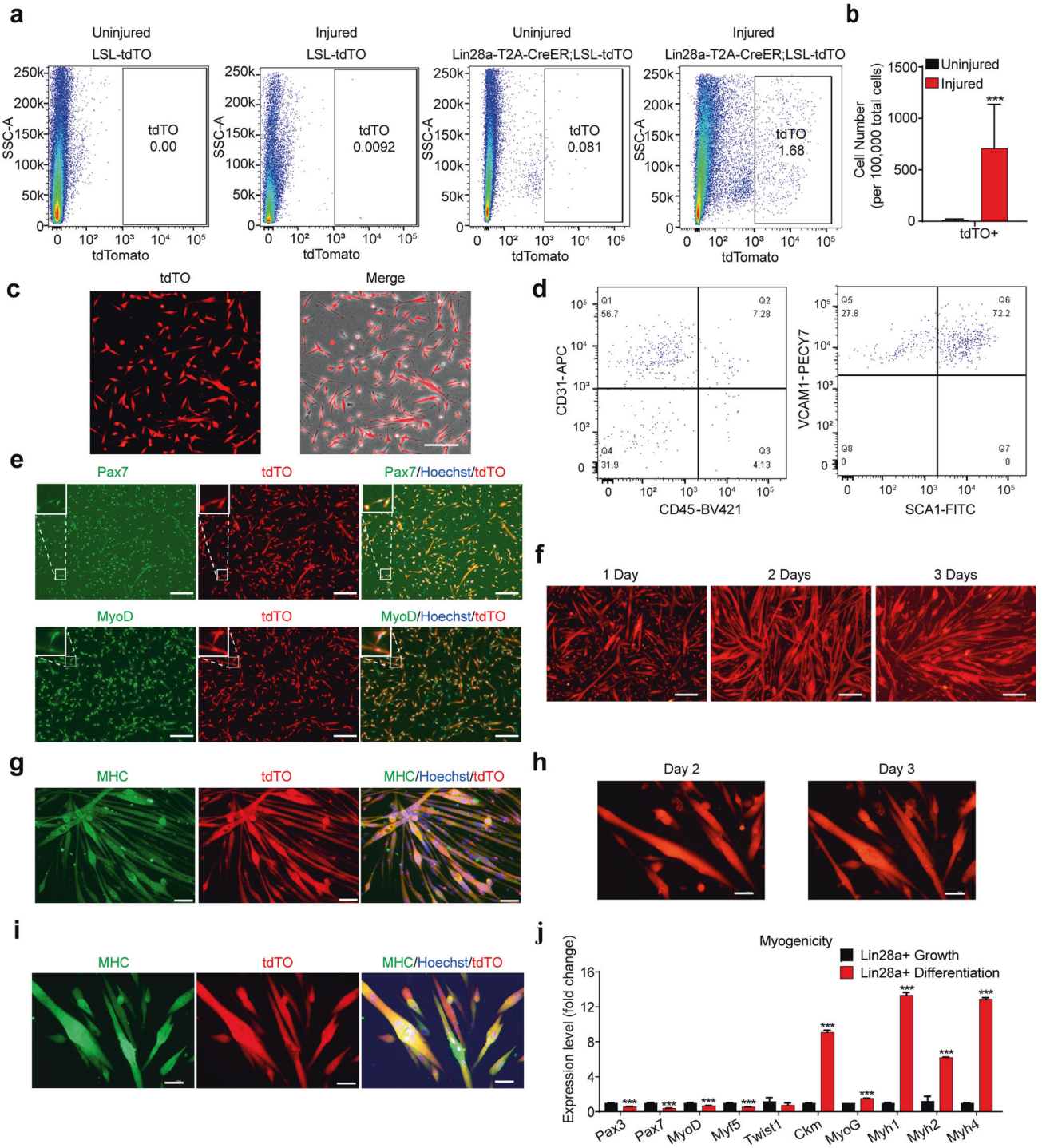

Fig. 3 **Lin28a$^+$ cells are MuSCs with robust myogenic capacity. a** Flow cytometry analysis for Lin28a-tdTO$^+$ cells in the uninjured and injured muscles of *Lin28a-T2A-CreER;LSL-tdTO* mice. The control groups were uninjured and injured *LSL-tdTO* mice. All the mice were injected with TMX, and harvested 14 days after injury. **b** Quantification of the number of tdTO$^+$ cells in injured or uninjured *Lin28a-T2A-CreER;LSL-tdTO* mice. $n = 6$ mice for each group. **c** Confocal microscopy on freshly FACS-isolated Lin28a-tdTO$^+$ cells. Scale bar, 200 μm. **d** Flow cytometry analysis for tdTO$^+$ cells. Cells were first labeled with antibodies conjugated with fluorescent dyes for CD31 (APC), CD45 (BV421), VCAM1 (PE), Sca1 (FITC). The Lin28a-tdTO$^+$ cells are mainly VCAM1$^+$CD31$^+$Sca1$^+$CD45$^-$ cells. **e** Immunofluorescence staining (green) revealed that most of the Lin28a-tdTO$^+$ cells cultured in GM become Pax7$^+$MyoD$^+$ progenitors within 24 h of culture in vitro. Scale bars, 250 μm. **f** Lin28a-tdTO$^+$ cells fused, differentiated and formed multinucleated myotubes starting at 1 and 2 days in myogenic DM. Scale bars, 500 μm. **g** MHC (green) and Hoechst (blue) staining revealed that the majority of Lin28a-tdTO$^+$ cells expressed MHC after differentiation into myotubes. Scale bars, 80 μm. **h** Single VCAM1$^+$CD31$^+$Sca1$^+$Lin28a-tdTO$^+$ cells all survived, proliferated, fused, differentiated and formed multinucleated myotubes at 2 and 3 days in DM. Scale bars, 40 μm. **i** MHC (green) and Hoechst (blue) staining revealed that all the VCAM1$^+$CD31$^+$Sca1$^+$Lin28a-tdTO$^+$ single cell-derived colonies expressed MHC after differentiation into myotubes. Scale bars, 40 μm. **j** qRT-PCR analysis revealed that myogenic differentiation-related genes, such as *MyoG*, *Ckm*, *Myh1*, *Myh2*, *Myh4*, were strongly activated, whereas myogenic progenitor-related genes, such as *Pax3*, *Pax7*, *MyoD*, *Myf5*, were significantly reduced, when Lin28a-tdTO$^+$ cells were cultured in myogenic DM, relative to undifferentiated Lin28a-tdTO$^+$ cells cultured in GM. ***$P < 0.001$.

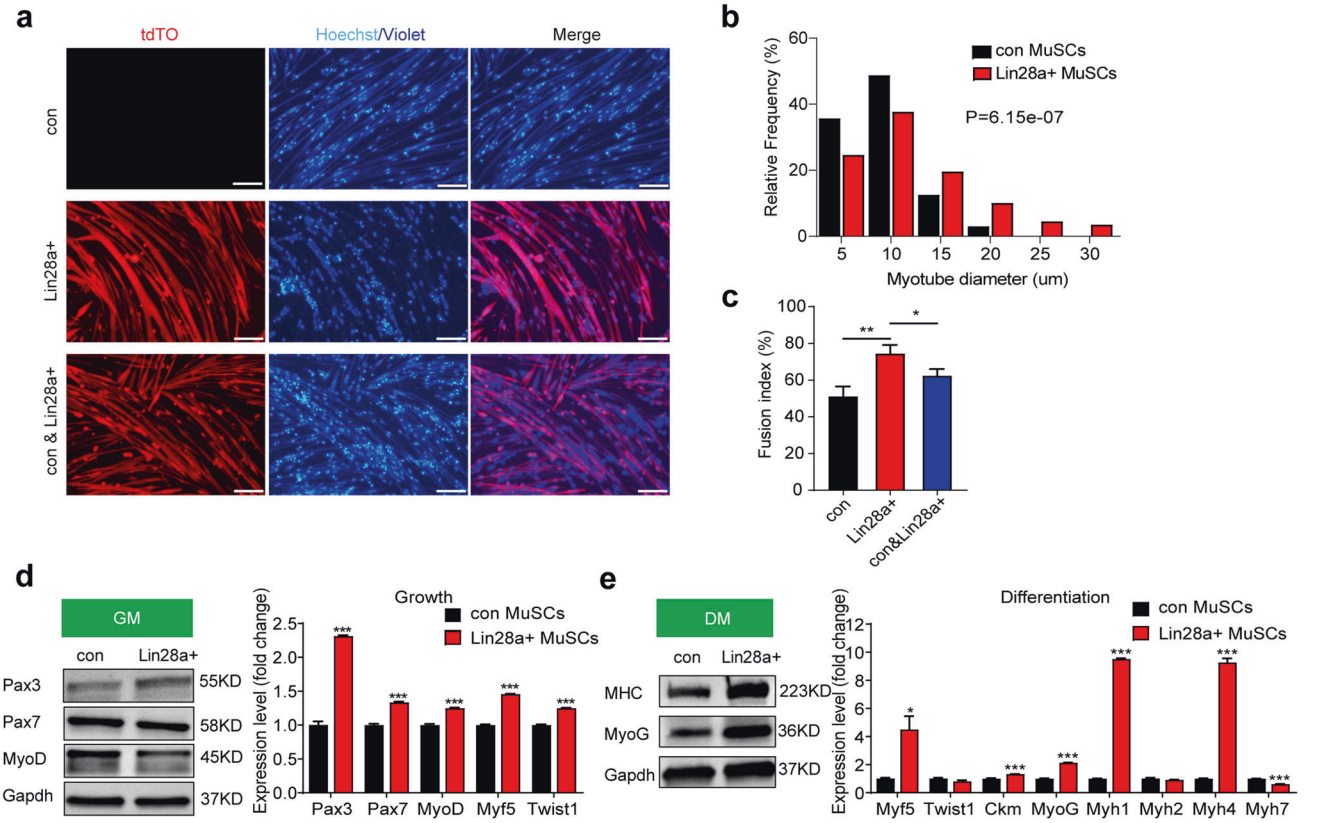

Fig. 4 Lin28a$^+$ MuSCs show enhanced myogenic potency in vitro. a Immunofluorescence images of conventional (con) MuSCs (CellTrace Violet-labeled), Lin28a-tdTO$^+$ cells, and a 1:1 mixture of con MuSCs with Lin28a-tdTO$^+$ cells, after FACS-isolation from the TA muscles of *Lin28a-T2A-CreER;LSL-tdTO* mice 14 days post injury followed by 36-h differentiation into myotubes. Scale bars, 100 μm. **b** Relative frequency distribution of the diameters of myotubes formed by the fusion of Lin28a-tdTO$^+$ cells and/or con MuSCs. For each bin, 200 myotubes were quantified. $P = 6.15 \times 10^{-7}$. **c** Quantification of the fusion index of these myotubes. For each group, at least three different fields were quantified. **d** Western blot analysis (left) for Pax3, Pax7 and MyoD protein expression in Lin28a$^+$ cells. qRT-PCR analysis (right) revealed expression levels of *Pax3*, *Pax7*, *MyoD*, *Myf5* and *Twist1* in Lin28a$^+$ cells relative to con MuSCs, when the cells were proliferated in GM. Gapdh served as the loading control. Unprocessed original scans of blots are shown in Supplementary information, Fig. S7. **e** Western blot analysis (left) for MHC and MyoG protein expression in Lin28a$^+$ cell-derived myotubes. qRT-PCR analysis (right) revealed expression levels of *Myf5*, *Twist1*, *Ckm*, *MyoG*, *Myh1/2/4/7* in Lin28a$^+$ cell-derived myotubes, relative to con MuSC-derived myotubes, when they were differentiated in DM. Gapdh served as the loading control. Unprocessed original scans of blots are shown in Supplementary information, Fig. S7. $^*P < 0.05$, $^{**}P < 0.01$, $^{***}P < 0.001$.

demethylated genes was highly enriched for cell migration- and angiogenesis-associated genes (Fig. 5d and Supplementary information, Fig. S5d), suggesting that Lin28a$^+$ MuSCs resembled embryonic limb progenitors which are highly migratory and pro-angiogenic.[36,37] However, Lin28a$^+$ MuSCs still showed an adult MuSC-like methylation pattern for the myogenic factor *Myf5*, unlike the Myf5$^+$Pax7$^+$ embryonic muscle progenitors (Fig. 5e). Overall, Lin28a$^+$ MuSCs were similar to adult Pax7$^+$ MuSCs in some aspects as expected, and also possessed embryonic-like features.

Transcriptomic profiles show that Lin28a$^+$ MuSCs are more dedifferentiated than Pax7$^+$ MuSCs

We then performed RNA-sequencing (RNA-seq) analysis to confirm the epigenetic similarities and differences between Lin28a$^+$ and Pax7$^+$ MuSCs. Transcriptomic hierarchical clustering ($n = 3$ mice each) showed that Lin28a$^+$ MuSCs differed from conventional Pax7$^+$ MuSCs (Fig. 6a). Volcano plot analysis showed that 78 genes were significantly upregulated (> 2-fold, $P < 0.05$), while 83 genes were significantly downregulated (> 2-fold, $P < 0.05$) (Fig. 6b). Amongst the upregulated genes are the p53 inhibitor *Mdm4*, the telomerase component *Tep1*, and 3 transcription factors in embryonic limb bud mesoderm progenitors:[38–42] *Meis2* (~27-fold), *Six1* (~10-fold), and *Eya4* (~3-fold) (Fig. 6c). These observations were also confirmed by low-protein-input capillary-based immunoassays (Fig. 6c). We also examined the expression of *Peg3* and *Pdgfra*,[6,7] markers of other known muscle-resident progenitors, and found no significant increase (Fig. 6d). In contrast, markers of myogenic terminal differentiation were amongst the most significantly downregulated genes, including the troponins and tropomyosins (Fig. 6e), confirming that Lin28a$^+$ MuSCs are more dedifferentiated relative to Pax7$^+$ MuSCs.

Consistently, pathway enrichment analysis showed that several stemness signatures were upregulated in Lin28a$^+$ MuSCs (Fig. 6f). Many stress response pathways were also upregulated in Lin28a$^+$ MuSCs: the pro-inflammatory stress responses mediated by TNF-NF-κB and IL6-STAT3, the unfolded protein response mediated by PERK, and the metabolic stress responses mediated by FoxO (Fig. 6f). In contrast, the Ca^{2+} signaling- and myogenic differentiation-related genes, all of which signify myogenic differentiation, were downregulated in Lin28a$^+$ MuSCs (Fig. 6f, g). Our analysis concluded that Lin28a$^+$ MuSCs, in comparison to conventional Pax7$^+$ MuSCs, show increased self-renewal, dedifferentiation and stress response signatures.

To further test whether these signatures merely correlate with *Lin28a* expression, or are due to *Lin28a* expression, we expressed *Lin28a* in conventional Pax7$^+$ MuSCs (Supplementary information, Fig. S6e), and repeated the transcriptomic analysis (Supplementary

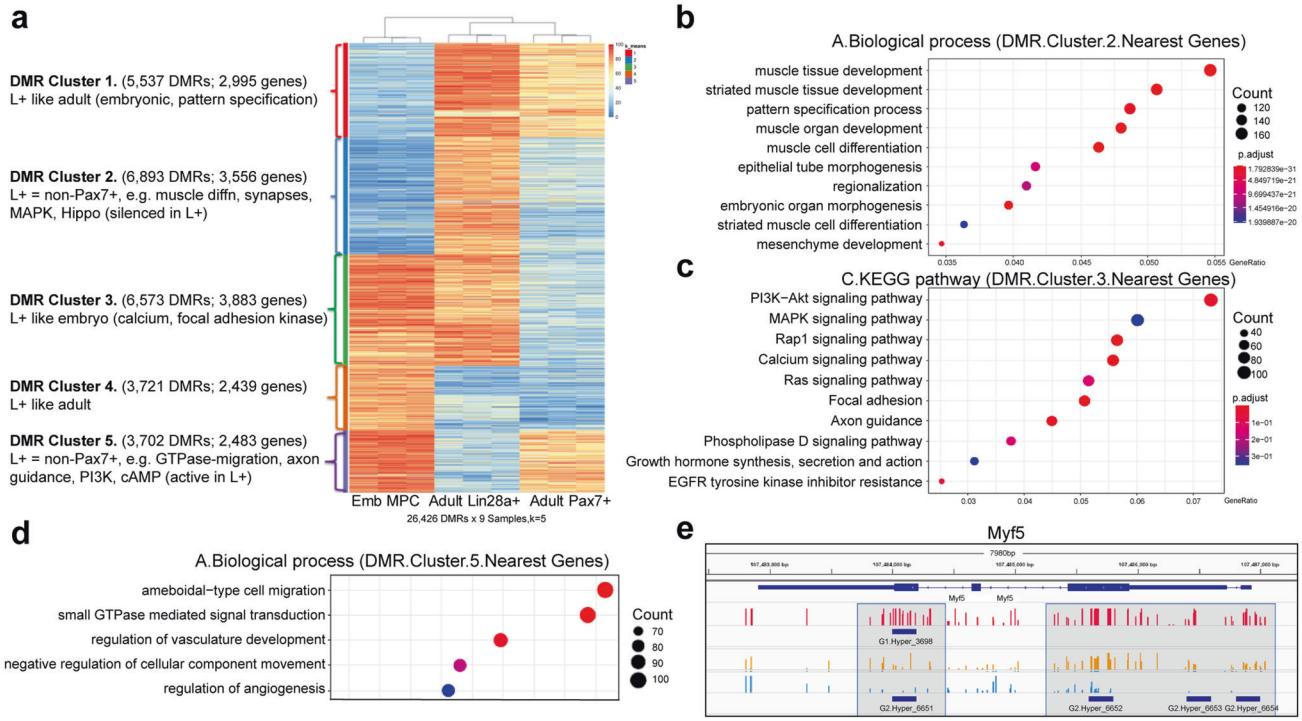

Fig. 5 Epigenomic profiles show that Lin28a$^+$ MuSCs resemble embryonic muscle progenitors. a Hierarchical clustering analysis (heatmap and dendrogram) for the DNA methylomes of freshly isolated embryonic muscle progenitors, adult Lin28a$^+$ MuSCs, and adult Pax7$^+$ MuSCs. $n = 3$ mice for each group. DMR differentially methylated region, Emb MPC embryonic muscle progenitors. **b** GO analysis of Cluster 2 in **a**. **c** KEGG analysis of Cluster 3 in **a**. **d** GO analysis of Cluster 5 in **a**. **e** CpG site methylation level in the region near the *Myf5* locus of adult Lin28a$^+$ MuSCs (red), adult Pax7$^+$ MuSCs (yellow), and embryonic muscle progenitors (blue). *Myf5* was heavily methylated in adult Lin28a$^+$ MuSCs, partially methylated in adult Pax7$^+$ MuSCs, and demethylated in embryonic muscle progenitors.

information, Fig. S6a). Gene set enrichment analysis (GSEA) showed that *Lin28a* overexpression led to increased stemness signatures such as Notch and Wnt signaling pathways, and E2F/mitosis/replication/cell cycle-related signatures (Supplementary information, Fig. S6b, c and Tables S1 and S2). In contrast, the myogenic differentiation signatures (Myogenic_Targets_of_*Pax3*; Striated_Muscle_Contraction) were downregulated (Supplementary information, Fig. S6b, c), indicating that *Lin28a* promotes the self-renewal capacity and dedifferentiation in MuSCs. Furthermore, compared with the empty vector control and conventional Pax7$^+$ MuSCs, the proliferative self-renewal capacity of *Lin28a*-overexpressing cells was enhanced (Fig. 6h, i), confirming the RNA-seq findings on stemness signatures. The RNA-seq findings on dedifferentiation were also confirmed by qRT-PCR (Fig. 6j, k), which showed that after *Lin28a* overexpression, genes related to differentiation such as *Ckm*, *MyoG*, *Myh1*, *Myh2*, *Myh4* decreased significantly in the MuSCs (Fig. 6j, k). We also tested whether the lineage potential of tdTO$^+$ cells was altered by *Lin28a* overexpression. We found that the overexpression of *Lin28a* enhanced some markers of osteogenic differentiation, significantly inhibited the capacity for adipogenic differentiation, and produced little effect on vascular cell differentiation (Supplementary information, Fig. S6d). These results suggest that the reactivation of *Lin28a* in cultured tdTO$^+$ cells can mimic the characteristics of freshly FACS-sorted Lin28a$^+$ cells in vivo, which also showed a weak capacity for osteogenesis but not adipogenesis nor vascular differentiation (Supplementary information, Fig. S3). Altogether, these results demonstrate that Lin28a functionally promotes the self-renewal of a dedifferentiated state in MuSCs.

Lin28a$^+$ MuSCs are necessary for efficient adult regeneration in vivo

To test the necessity of Lin28a$^+$ MuSCs in normal regeneration, we bred *Lin28a-CreER* mice with *Rosa26-DTA* mice, such that adult Lin28a$^+$ cells would be ablated by intracellular diphtheria toxin A in LD (*Lin28a-CreER;Rosa26-DTA*) mice after tamoxifen (TMX) injection. It was visually appreciated that the resolution of necrotic and inflamed muscle tissue was worse in LD mice than that in control DTA (*Rosa26-DTA*) mice by day 11 post injury (Fig. 7a). Quantification of centrally nucleated and eMHC-positive regenerating myofibers, Pax7$^+$ MuSCs, and assessment of myofiber diameters, all indicated that the regeneration was delayed in LD mice (Fig. 7b–d). We performed immunofluorescence staining on the skeletal muscle sections, and found that there were significantly fewer Pax7$^+$ MuSCs and Pax3$^+$ MuSCs in LD mice than in control DTA mice by day 11 post injury, suggesting that the rare Lin28a$^+$ MuSCs are required for the proper self-renewal of the MuSC pool in adulthood (Fig. 7e, f).

Injury-inducible Lin28a$^+$ MuSCs are sufficient to enhance adult regeneration

Our experiments led us to ask whether conversion of conventional adult Pax7$^+$ MuSCs into Lin28a$^+$ MuSCs in vivo can also enhance muscle regeneration. To this end, we constructed an *NF-κB promoter-LSL-Lin28a* transgenic mouse (no. *Mt190*), and bred it with *Pax7-CreER* mice to obtain PM (*Pax7-CreER;Mt190*) mice that can conditionally express *Lin28a* in Pax7$^+$ MuSCs only after TMX injection in adulthood and during muscle injury-induced inflammation, and further shut it off after inflammatory signaling is resolved.

Following the same schedule of TMX injection and injury as our lineage-tracing experiments (Fig. 1a), we tested the regeneration ability of 8-month-old PM mice after double-blinded cryoinjury tests on the TA muscles. By day 4 post injury, the overexpression of *Lin28a* in both Pax7$^+$ MuSCs and muscles of injured PM mice were confirmed by qRT-PCR and low-protein-input capillary-based immunoassays; and we found that injury slightly increased *Lin28a*

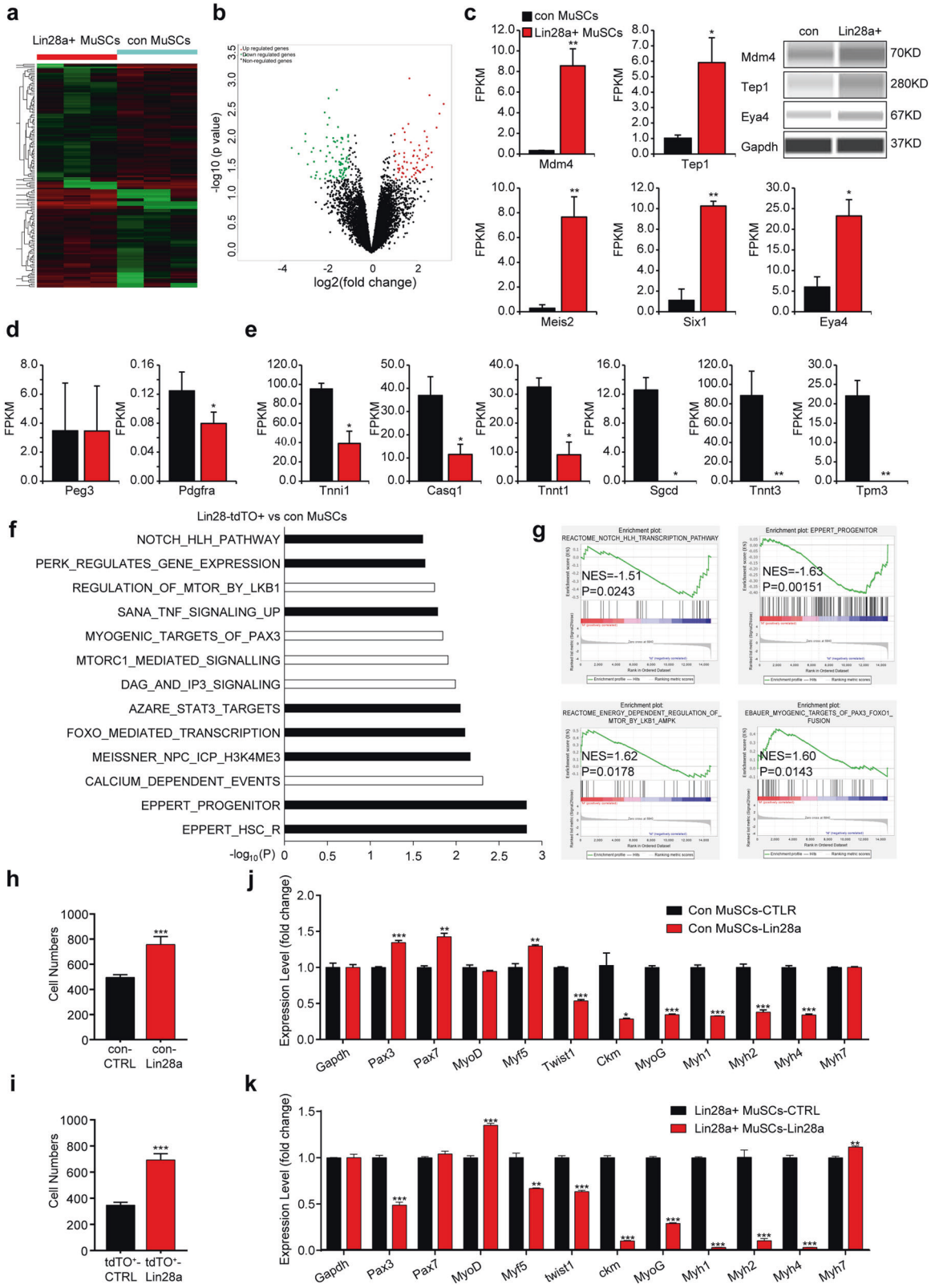

in *Pax7-CreER* (PC) mice (~56-fold) while significantly upregulating *Lin28a* in PM mice (~586-fold) (Fig. 8a). By day 7 post injury, it was visually appreciated that the resolution of necrotic and inflamed muscle tissue was more efficient in PM mice than in control PC mice (Fig. 8b). Histological analysis revealed that the TA muscles of PM mice had smaller necrotic zones and larger regenerative zones with centrally nucleated myofibers by day 7 post injury (Fig. 8c). These results suggested that inflammation-induced Lin28a in Pax7^{+} MuSCs accelerated muscle regeneration. Indeed, at the end of 11 days of regeneration, the regenerated myofibers in PM mice were significantly larger than those in control PC mice (Fig. 8d), and had further matured beyond eMHC-positive myofibers (Fig. 8e).

Fig. 6 Transcriptomic profiles show that *Lin28a* promotes MuSC dedifferentiation. a Hierarchical clustering analysis for the transcriptomes of freshly isolated Lin28a$^+$ MuSCs and conventional (con) Pax7$^+$ MuSCs. $n = 3$ mice for each group. **b** Volcano plot analysis for differentially expressed genes in Lin28a$^+$ MuSCs, relative to con Pax7$^+$ MuSCs. Red, upregulated > 2-fold and $P < 0.05$. Green, downregulated > 2-fold and $P < 0.05$. **c** Expression levels of *Mdm4*, *Tep1* and three primitive limb mesodermal progenitor transcription factors, *Meis2*, *Six1*, *Eya4* in Lin28a$^+$ MuSCs relative to con Pax7$^+$ MuSCs. FPKM fragments per kilobase of transcript per million mapped reads. Right: low-protein-input capillary-based immunoassays for Eya4, Tep1 and Mdm4 protein expression. Gapdh served as the loading control. **d** Expression levels of markers expressed in other muscle-resident Pax7-independent progenitors, *Peg3* and *Pdgfra*, in Lin28a$^+$ MuSCs relative to con Pax7$^+$ MuSCs. **e** Expression levels of myogenic terminal differentiation markers, including many troponins (*Tnni1*, *Tnnt1*, *Tnnt3*), calsequestrin (*Casq1*), sarcoglycan (*Sgcd*), and tropomyosin (*Tpm3*), in Lin28a$^+$ MuSCs relative to con Pax7$^+$ MuSCs. **f** Signatures enriched in Lin28a$^+$ MuSCs, compared with con Pax7$^+$ MuSCs, as identified by GSEA. Upregulated pathways are shown with black columns, and downregulated pathways are shown with white columns. **g** Representative GSEA profiles with the normalized enrichment scores (NESs) and nominal *P* values shown. **h**, **i** Cell proliferation rate of con MuSCs (**h**) and Lin28a-tdTO$^+$ MuSCs (**i**), after being infected with retroviruses expressing either empty vector (CTRL) or *Lin28a*. **j**, **k** qRT-PCR for myogenic differentiation markers in con MuSCs (**j**) or Lin28a-tdTO$^+$ MuSCs (**k**) which overexpressed *Lin28a*, relative to con MuSCs or Lin28a-tdTO$^+$ MuSCs with the empty vector (CTRL). Data are means ± SEM. $n = 3$ independent experiments. $^*P < 0.05$, $^{**}P < 0.01$, $^{***}P < 0.001$.

In order to determine whether MuSC self-renewal was affected, we performed immunofluorescence staining on the TA muscles. We found that, consistent with our epigenomic/transcriptomic observations that *Lin28a* rejuvenated mouse adult MuSCs, the numbers of Pax7$^+$ MuSCs and MyoD$^+$ myoblasts were significantly larger in the TA muscles of PM mice than in control PC mice (Fig. 8f–h). These in vivo results confirmed that the injury-induced expression of *Lin28a* in Pax7$^+$ MuSCs is sufficient to promote their self-renewal and proliferation, thereby enhancing skeletal muscle regeneration in response to injuries.

DISCUSSION

Lin28a is mainly expressed during embryonic development and declines with development.[22,43] However, its expression and function in mammalian adult tissue regeneration had remained elusive hitherto. Through post-transcriptional lineage tracing, we identified a rare alternative group of adult Lin28a$^+$ MuSCs which replenish adult Pax7$^+$ MuSCs, and show enhanced regenerative potential. Lin28a$^+$ MuSCs possess surface marker, epigenomic and transcriptomic profiles that suggest they resemble embryonic limb bud mesoderm progenitors, expressing transcription factors such as *Meis2*, *Six1*, *Eya4* and *Pax3*, compared to adult Pax7$^+$ MuSCs. *Pax3* regulates somite and limb muscle development in collaboration with a genetic network of *Six* and *Eya* family members,[36,40–42,44–47] whereas *Lin28a* was only known to be expressed in limb buds during embryogenesis.[48,49] Consistent with these reports, we traced Lin28a$^+$ cells during embryonic limb development, and found migrating Lin28a$^+$ limb muscle progenitor cells that also gave rise to limb bud myofibers. Mechanistically, *Lin28a* upregulates many stemness, self-renewal and stress-responsive pathways, while suppressing differentiation markers in the MuSCs, further supporting the notion that *Lin28a* can maintain some reserve adult MuSCs in a dedifferentiated embryonic-like state.

To confirm these findings in vivo, we induced *NF-κB* promoter-driven *Lin28a* in Pax7$^+$ MuSCs after cryoinjury, and found that Lin28a$^+$ MuSCs were sufficient to promote muscle regeneration in vivo. Moreover, ablation of Lin28a$^+$ MuSCs impaired the self-renewal of the MuSC pool. These, together with the lineage-tracing results, demonstrate that Lin28a$^+$ MuSCs replenish a substantial fraction of adult Pax7$^+$ MuSCs after injury. Thus, Lin28a$^+$ MuSCs are required for the long-term self-renewal of adult MuSC pools and efficient adult muscle regeneration in vivo. This extends our knowledge on Lin28a, which had been primarily thought to just specifically mark embryonic cells or induced pluripotent stem cells (iPSCs).[17,50,51] Moreover, given that Lin28a$^+$ MuSCs differ from Pax7$^+$ MuSCs, our findings will expand our understanding of adult stem cell heterogeneity to advance regenerative medicine.[34,52,53]

Through lineage tracing and dissection of the functional role of *Lin28a* in MuSCs and muscle regeneration, our study has identified an endogenous heterochronic factor that coordinates stemness and stress response pathways to maintain some adult stem cells in an embryonic-like state, thus ensuring the long-term self-renewal of the adult MuSC pools. These findings might have important implications for our understanding of how developmental timing and biological aging are interrelated,[33,54,55] and why juvenile regeneration tends to be stronger than adult regeneration.[56,57] Organismal aging is a multifarious collection of black box processes that have confounded scientists for centuries. While the 4 Yamanaka pluripotency factors (Oct4, Sox2, Klf4, c-Myc) can completely reset aging clocks back to zero,[21,32] there is a huge unmet need for a single molecule that can partially dial back aging without lineage reprogramming or teratoma formation. In contrast to adult and aged animals, where senescent stem cells fail to regenerate properly after injury, juvenile animals manifest robust regeneration without tumorigenesis.[58] Mammalian fetuses and neonates can regenerate multiple tissues more robustly than adult mammals.[59–61] Young fish and larval invertebrates can regenerate tissues more robustly than aged fish and adult invertebrates. This conserved relationship between juvenility and tissue regeneration was first discussed by Charles Darwin,[56,57] but the precise mechanisms that underlie juvenile regeneration has remained unclear. Given that our findings on Lin28a$^+$ stem cells provide cellular-level insights into how mammals maintain juvenile stem cells, we believe our findings will motivate new efforts to fully understand juvenility.

MATERIALS AND METHODS

Transgenic mice

The targeting strategy for the generation of *Lin28a-T2A-CreERT2* mice is shown in Supplementary information, Fig. S1a, b. In the construction of the donor vector, the genomic fragment from the third exon to the last intron of mouse *Lin28a*, and the genomic fragment in the *Lin28a* 3′UTR, were used as the two homology arms, respectively. An *Frt-Neo-Frt-last exon-2A-CreERT2* expression cassette was inserted between the two arms to obtain the donor vector. The donor vector was electroporated into mouse embryonic stem cells. Through homologous recombination, the donor vector could insert the *Frt-Neo-Frt-2A-CreERT2* fragment between the last exon and 3′UTR of *Lin28a*. With G418 selection, the targeted ES cell clones were selected. Next, the *Frt-Neo-Frt* expression cassette in selected ES cell clones was deleted and the resultant ES cells were injected into C57BL/6 albino embryos. The original animal was identified by its coat color, and its germline transmission was confirmed by reproduction with female C57BL/6 mice and subsequent genotyping. In the construction of the targeting vector to generate *NF-κB-LSL-lin28a-T2A-luc* (no. Mt190) mice, the NF-κB response element and its downstream TAp promoter (the minimal TA promoter of the herpes simplex virus)[62] were inserted upstream of a fragment of *LSL*. The *LSL* fragment contains 2 *LoxP* sites and 3 *SV40 late polyA* fragments between the 2 *LoxP* sites. Located downstream of the *LSL* fragment is the CDS of *Lin28a* which is tagged with *T2A-luc* (firefly luciferase reporter gene). The targeting vector was integrated into the *H11* site of C57BL/6 mice as previously reported to ensure the specificity of the NF-κB response element.[63] *Rosa26-CAG-tdTO* mice ((*ROSA)*

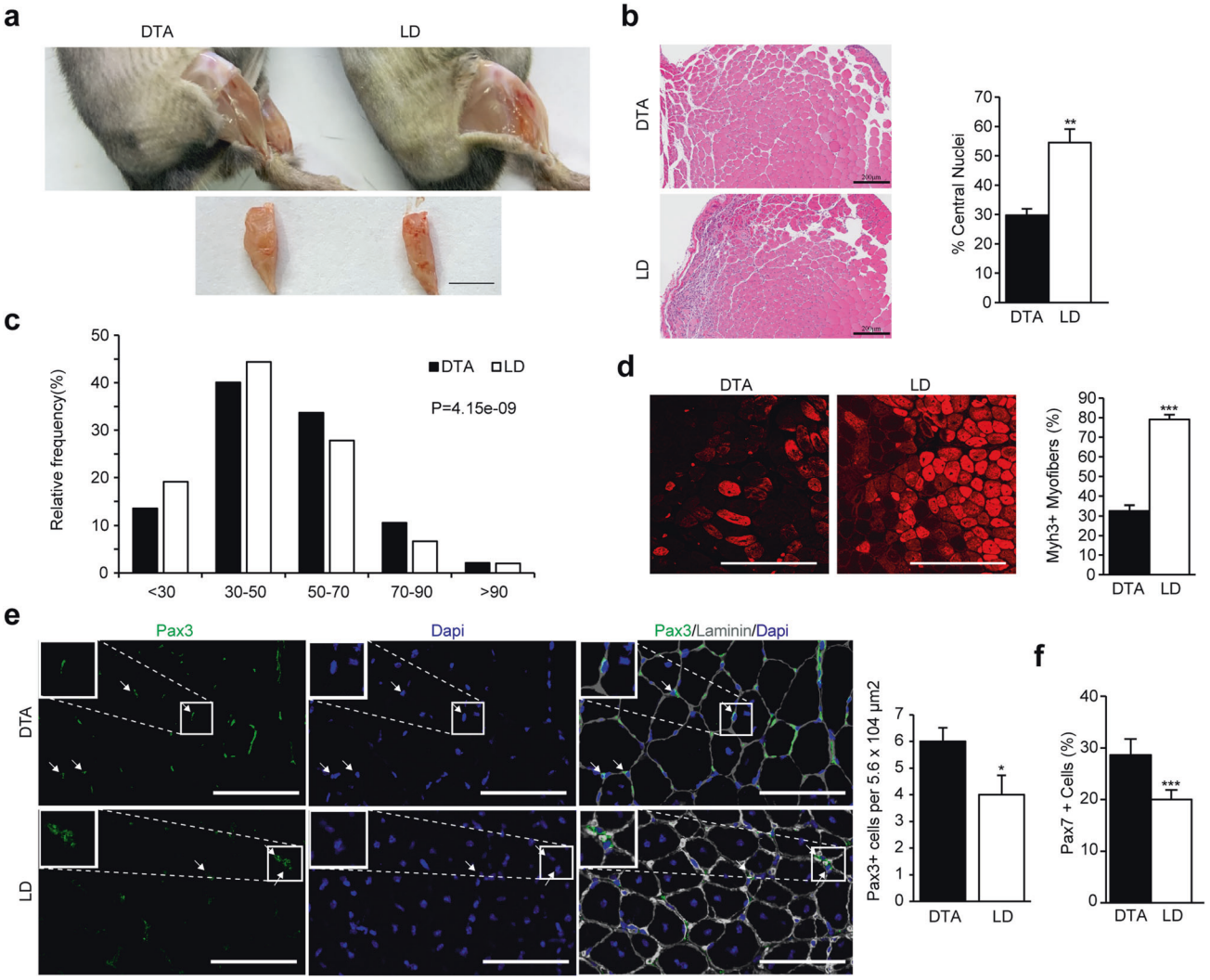

Fig. 7 Lin28a$^+$ MuSCs are necessary for efficient muscle regeneration. a Photographs show the resolving of muscle inflammation and muscle regeneration in the TA muscles of adult *Rosa26-DTA* (DTA) and adult *Lin28-CreER;Rosa26-DTA* (LD) mice on day 11 post injury. Scale bar, 5 mm. **b** Hematoxylin and eosin (H&E) staining of TA muscle sections of DTA and LD mice, on day 11 post injury. Scale bars, 200 μm. Right: quantification of the percentage of myofibers that were regenerating with central nuclei. For each muscle section, at least seven different fields were quantified. **c** Relative frequency distribution of the Feret diameters of myofibers in the TA muscles of DTA vs LD mice. **d** Immunofluorescence staining for embryonic MHC (Myh3) expression in the injured TA muscles from LD mice relative to DTA mice on day 11 post injury. Right: quantification of the percentage of Myh3$^+$ myofibers. For each muscle section, at least seven different fields were quantified. Scale bars, 200 μm. **e** Cryosections of the TA muscles of DTA and LD mice that were cryoinjured and harvested on day 11 post injury. Muscle sections were co-stained for Pax3 (green), laminin (white) and DAPI (blue). White arrows indicate Pax3$^+$ cells. Right: quantification of the Pax3$^+$ cell numbers in DTA and LD mice. For each muscle section, at least five different fields were quantified and averaged. Scale bars, 100 μm. **f** Quantification of the percentage of Pax7$^+$ MuSCs in the TA muscles of DTA and LD mice after cryoinjury. For each muscle section, at least seven different fields were quantified. *$P < 0.05$, **$P < 0.01$, ***$P < 0.001$.

26Sor$^{tm14(CAG-tdTomato)Hze}$, stock no. 007914) and *Rosa26-DTA* mice ((*ROSA)26Sor*$^{tm1(DTA)Lky}$, stock no. 009669) were obtained from the JAX laboratory. All animal procedures were approved by the Institute of Zoology and the Institute of Stem Cell and Regenerative Medicine, Chinese Academy of Sciences.

TMX and cryoinjury treatment

TMX (Sigma-Aldrich) was dissolved at 20 mg/mL in corn oil, and 100 mg/kg of TMX was administered by intraperitoneal injection into 6-month-old mice, as schematized in Fig. 1a. For cryoinjury, all mice were anesthetized using isoflurane. The skin was cut open with a scalpel to expose the TA muscle. A steel probe with a diameter of 4 mm was cooled in liquid nitrogen and placed on the TA muscle for 10 s, twice. Subsequently, the skin incision was closed with surgical sutures immediately and betadine was applied to the wound to prevent infection after injury. The TA and SOL muscles were harvested 7–14 days after cryoinjury. One thousand tdTO$^+$ cells and 1×10^6 GFP$^+$ LTS progenitors were injected into the TA muscle 1 day post injury for all orthotopic transplantation experiments.

Immunofluorescence analysis

After skeletal muscles were harvested, they were fixed in 4% paraformaldehyde at 4 °C for 1 h. Tissues were then switched to 20% sucrose/ddH_2O at 4 °C overnight, and after this, they were freeze-embedded with OCT and sectioned with 10-μm thickness. Before immunostaining, frozen slides were fixed in methanol for 10 min at room temperature and then washed with PBS. Next, slides immersed in citrate antigen retrieval solution (ab208572) were placed in a pressure cooker. Then, slides were treated with 0.3% Triton X-100/PBS at room temperature for 15 min, followed by incubation with mouse IgG-blocking solution (M.O.M. kit, Vector Lab) at room temperature for 1 h, according to the manufacturer's instructions. Slides were incubated with primary antibodies diluted in 0.3% Triton X-100, 5% goat serum/PBS at 4 °C overnight. The next morning, slides were washed with PBS and

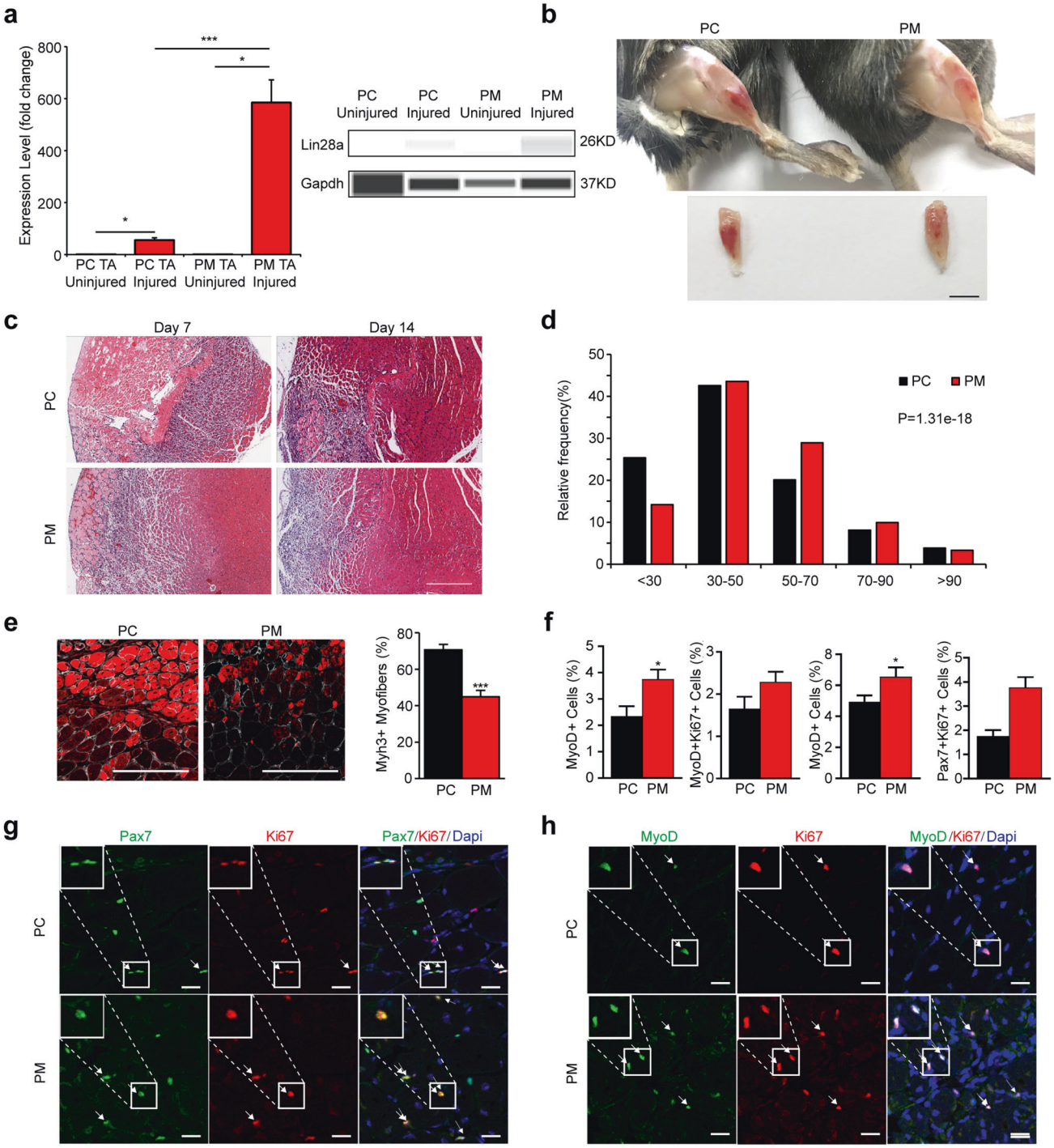

Fig. 8 Injury-inducible *Lin28a* is sufficient to enhance adult muscle regeneration. a qRT-PCR analysis of *Lin28a* in TA muscles of injured *Pax7-CreER* (PC) and *Pax7-CreER;NF-κB-LSL-Lin28a* (PM) mice, relative to uninjured PC mice. Right: low-protein-input capillary-based immunoassays for Lin28a protein expression in $Pax7^+$ MuSCs of TA muscles of the above mice. Gapdh protein was used as the loading control. **b** Photographs showing the resolving of muscle inflammation and muscle regeneration in the TA muscles of 8-month-old PC and PM mice on day 7 post injury. Scale bar, 5 mm. **c** H&E staining of TA muscle sections of PM mice, relative to PC mice, on days 7 and 14 post injury. Scale bar, 300 μm. **d** Relative frequency distribution of the Feret diameters of myofibers in the TA muscles of PC vs PM mice. **e** Immunofluorescence staining for embryonic MHC (Myh3) expression in the injured TA muscles from PM mice relative to PC mice, on day 11 post injury. Right: quantification of the percentage of $Myh3^+$ myofibers. For each muscle section, at least seven different fields were quantified. Scale bars, 200 μm. **f** Quantification of the percentage of each type of MuSC and myoblast, after injured TA muscle sections were immunostained for Ki67, MyoD and Pax7. For each muscle section, at least seven different fields were quantified. **g** Immunofluorescence staining for Pax7 and Ki67 expression in the damaged TA muscles from PM mice, relative to PC mice. White arrows indicate $Pax7^+Ki67^+$ cells. Scale bars, 20 μm. **h** Immunofluorescence staining for MyoD and Ki67 expression in the injured TA muscles from PM mice, relative to PC mice. White arrows indicate $MyoD^+Ki67^+$ cells. Scale bars, 20 μm. $^*P < 0.05$, $^{***}P < 0.001$.

incubated with secondary antibodies diluted in 0.3% Triton X-100, 5% goat serum/PBS at room temperature and protected from light for 1 h. Slides were then washed with PBS and sealed with glycerin with DAPI. For immunofluorescence assays, the following antibodies were used: anti-Pax7, anti-Pax3, anti-myosin I (BA-D5), anti-myosin IIa (SC-71) (all from Developmental Studies Hybridoma Bank (DSHB), 1:10), anti-IIx, anti-IIb (fast myosin, Abcam, ab91506), anti-laminin (Sigma-Aldrich, # L9393, 1:500), anti-desmin (Abcam, ab32362, 1:200). Alexa Fluor secondary antibodies were used according to the manufacturer's instructions. Images were taken on a Nikon confocal microscope or PerkinElmer Vectra Polaris. For Pax3 and Pax7 staining, isotype control antibodies mouse IgG2a isotype control (CST, 61656S) and mouse IgG1 isotype control (R&D, MAB002) were used to confirm the fidelity of Pax3 and Pax7 staining (Supplementary information, Fig. S2d). For muscle fiber type identification, type I and IIa myofibers were identified by antibodies against myosin I (BA-D5) and myosin IIa (SC-71) directly; type IIb myofibers were identified by light staining with fast myosin antibody (Abcam, ab91506); type IIx myofibers were identified by intense staining with fast myosin antibody (Abcam, ab91506) but absence of staining with myosin IIa antibody (SC-71).

FACS analysis

Following the same schedule of TMX injection and injury as our lineage-tracing experiments (Fig. 1a), Lin28a-tdTO$^+$ mononucleated cells were isolated at the same time (14 days post injury) from the hindlimb muscles of uninjured or injured littermates. Conventional adult Pax7$^+$ MuSCs and Lin28a-tdTO$^+$ cells were isolated from the same mice, where the former were isolated by FACS as the VCAM1$^+$CD45$^-$CD31$^-$Sca1$^-$ population as described previously,[31] and the latter were isolated as tdTO$^+$ or VCAM1$^+$CD45$^-$CD31$^+$Sca1$^+$tdTO$^+$ cells. For embryonic Pax7$^+$ muscle progenitors,[27] pregnant *Pax7-CreER;LSL-tdTO* female mice were injected with TMX at 11.5 days post coitum and the embryos were harvested at E12.5. After dissection, embryos were used for Pax7-tdTO$^+$ embryonic muscle progenitor isolation. Mononucleated cells were rapidly separated from minced uninjured or cryoinjured muscles, and enzymatically digested as previously described.[31] Following separation, single cells from each mouse (~10^7 cells) were resuspended in 500 µL PBS/10% FBS/3 mM EDTA, then incubated on ice for 40 min with the following fluorophore-conjugated antibodies: APC-CD31 (clone MEC13.3), FITC-Sca1 (clone E13-161.7), VCAM1-biotin (clone 429) (all from Biolegend, 1:100), BV421-CD45 (Becton Dickinson, clone 30-F11, 1:250), and 20 min with PE-Cy7 streptavidin (BioLegend, Cat# 405206, 1:100). Fresh cells from wild-type mice stained with the same antibodies were used as the tdTomato FMO control. Unstained cells isolated from wild-type mice were used as unstained controls. Cells were analyzed on the FACSAria Fusion Flow cytometer (Becton Dickinson, USA), and FACS data were analyzed using FlowJo Software (TreeStar). Values of FACS analysis were averaged from more than five independent experiments.

Cell culture and myogenesis, adipogenesis and osteogenesis in vitro

After FACS, Lin28a$^+$ and conventional Pax7$^+$ MuSCs were cultured in Matrigel-coated plates. All cells were incubated at 37 °C, 5% CO_2 in GM, comprising DMEM/F-12 (Gibco) with 20% fetal bovine serum (FBS) (GE Healthcare), 1% L-glutamine (Gibco) and 1% penicillin-streptomycin (Gibco). At each passage, after reaching 80% confluence, cells were trypsinized and diluted at 1:4. Differentiation was initiated by replacing GM with DM, which comprised DMEM/F-12, 2% KnockOut Serum Replacement (Gibco), 1% L-glutamine (Gibco) and 1% penicillin-streptomycin (Gibco), when the cells were cultured to 80%–100% confluent. For fusion comparison experiments, conventional MuSCs stained with CellTrace Violet (Thermo Fisher, C34557), Lin28a$^+$ cells and 1:1 mixed cells were cultured in GM and then switched to DM to induce myotube formation, respectively. To quantify the cell proliferation rate, 4×10^4 cells were seeded in one gelatin-coated well of a 6-well plate (Falcon) with GM. After proliferating for 2 days, Hoechst 33342-stained cells in 5 random fields of each well, captured by a Nikon fluorescence microscope at 4× magnification, were automatically counted with an ImageJ script. For directed differentiation, freshly sorted Lin28a$^+$ cells were grown in GM for 3 days and subsequently differentiated in myotube-, adipocyte-, endothelial cell- or osteoblast-conditioned medium. For myotube differentiation, the GM was replaced with DM for 2–3 days. Cells were then immunostained for MyoG (Santa Cruz Biotechnology, sc-12732, 1:100) and MHC (DSHB, clone MF20, 5 µg/mL) to visualize differentiated myotubes. For adipocyte, endothelial cell and osteoblast differentiation, cells were treated and detected by staining as previously described.[64]

Immunostaining of cultured cells

For immunostaining, cells grown on plates were fixed with 4% paraformaldehyde at room temperature for 15 min and subsequently permeabilized with 0.3% Triton X-100/ PBS. Cells were blocked in 10% goat serum diluted in 0.1% Triton X-100/PBS at room temperature for 1 h. Primary antibodies were diluted in 1% goat serum/0.1% Triton X-100 and incubated at 4 °C overnight. Cells were washed, and then incubated with secondary antibodies diluted in 1% goat serum/0.1% Triton X-100 at room temperature for 1 h. Nuclei were stained with Hoechst 33342 (1:2000 in PBS) at room temperature for 10 min. Primary antibodies include: anti-Pax3 (DSHB, 1:20), anti-Pax7, (DSHB, 1:20), anti-MyoD (Santa Cruz Biotechnology, sc-377460, 1:100), anti-MyoG (Santa Cruz Biotechnology, sc-12732, 1:100), anti-MHC (DSHB, clone MF20, 5 µg/mL). MYHC-IIb eFluor 660 (Thermo Fisher, 50-6503-32, 1:100), anti-α-actinin (Santa Cruz, sc-7453, 1:500). Fusion index was calculated as a ratio of the number of tdTO$^+$ or MuSC nuclei within a multinucleated myotube to the total number of tdTO$^+$ or MuSC nuclei. A minimum of 4 independent microscopic fields were used for each group over three independent differentiation experiments at 24 h and 36 h in DM.

Nucleic acid isolation and sequencing

Total DNA and RNA were isolated according to the manufacturer's instructions (Invitrogen). DNA and RNA quality was verified by the Agilent 2100 Bioanalyzer. RNA quantity was verified by the Qubit RNA assay kit. cDNA libraries were constructed using the NEBNext Ultra RNA Library Prep Kit for Illumina. Deep sequencing was performed using Illumina Novaseq-6000.

qRT-PCR analysis

Total RNA was extracted from sorted cells with Trizol (Invitrogen) following the manufacturer's instructions. From this RNA, cDNA was reverse-transcribed with PrimeScript RT reagent Kit (Takara, RR047B). The resulting cDNA was diluted at 1:5 before qPCR was performed with qPCR SYBR Green Mix. qRT-PCR primer sequences were obtained from OriGene. With the resulting cDNA libraries, qRT-PCR was performed using the ABI Prism 7900HT (Applied Biosystems) according to the manufacturer's instructions.

Western blot analysis and low-protein-input capillary-based immunoassays

Proteins were extracted with RIPA buffer supplemented with protease inhibitor cocktails I and II (Sigma) and phosphatase inhibitor cocktail set III (Calbiochem). Proteins were quantified with Pierce BCA protein assay kit (Thermo Fisher) and analyzed with a Sunrise Tecan plate reader. After separated by SDS-PAGE electrophoresis and electro-transferred onto PVDF membranes, proteins were detected with the following primary antibodies and concentrations: anti-Lin28a (1:1000, CST), anti-Pax7 (0.28 µg/mL, DSHB), anti-Pax3 (0.31 µg/mL, DSHB), anti-MyoD (1:1000, Santa Cruz Biotechnology), anti-MHC (0.23 µg/mL, DSHB), anti-MyoG (1:1000, Santa Cruz Biotechnology), anti-Cre (1:1000, Millipore), anti-Gapdh (1:1000, CST). Low-input protein detection was performed using an automated capillary electrophoresis system (Simple Western system and Compass software, ProteinSimple) on 10,000 FACS-isolated cells. Wes Separation Capillary Cartridges for 12–230 kDa (ProteinSimple) were used for Lin28a (Figs. 1d and 8a), Mdm4 (1:100, Proteintech), Tep1 (1:100, Origene), Eya4 (1:1000, ProteinTech).

Statistical analysis

All statistical analyses were performed using GraphPad Prism 6 (GraphPad Software). Data are presented as means ± SEM. Differences between groups were tested for statistical significance by using the two-sample *t*-test. $P < 0.05$ was considered significant. The number of biological (non-technical) replicates for each experiment is indicated in the figure legends.

REFERENCES

1. Mauro, A. Satellite cell of skeletal muscle fibers. *J. Biophys. Biochem. Cytol.* **9**, 493–495 (1961).
2. Yin, H., Price, F. & Rudnicki, M. A. Satellite cells and the muscle stem cell niche. *Physiol. Rev.* **93**, 23–67 (2013).
3. von Maltzahn, J., Chang, N. C., Bentzinger, C. F. & Rudnicki, M. A. Wnt signaling in myogenesis. *Trends Cell Biol.* **22**, 602–609 (2012).
4. Rossi, G. & Messina, G. Comparative myogenesis in teleosts and mammals. *Cell Mol. Life Sci.* **71**, 3081–3099 (2014).

5. Kuang, S., Chargé, S. B., Seale, P., Huh, M. & Rudnicki, M. A. Distinct roles for Pax7 and Pax3 in adult regenerative myogenesis. *J. Cell Biol.* **172**, 103–113 (2006).
6. Joe, A. W. B. et al. Muscle injury activates resident fibro/adipogenic progenitors that facilitate myogenesis. *Nat. Cell Biol.* **12**, 153–163 (2010).
7. Mitchell, K. J. et al. Identification and characterization of a non-satellite cell muscle resident progenitor during postnatal development. *Nat. Cell Biol.* **12**, 257–266 (2010).
8. Fry, C. S. et al. Inducible depletion of satellite cells in adult, sedentary mice impairs muscle regenerative capacity without affecting sarcopenia. *Nat. Med.* **21**, 76–80 (2015).
9. McCarthy, J. J. et al. Effective fiber hypertrophy in satellite cell-depleted skeletal muscle. *Development* **138**, 3657–3666 (2011).
10. Kuang, S., Kuroda, K., Le Grand, F. & Rudnicki, M. A. Asymmetric self-renewal and commitment of satellite stem cells in muscle. *Cell* **129**, 999–1010 (2007).
11. Walker, D. K. et al. PAX7^{+} satellite cells in young and older adults following resistance exercise. *Muscle Nerve* **46**, 51–59 (2012).
12. Christensen, J. L. & Weissman, I. L. Flk-2 is a marker in hematopoietic stem cell differentiation: a simple method to isolate long-term stem cells. *Proc. Natl. Acad. Sci. USA* **98**, 14541–14546 (2001).
13. Horvitz, H. R. & Sulston, J. E. Isolation and genetic characterization of cell-lineage mutants of the nematode *Caenorhabditis elegans*. *Genetics* **96**, 435–454 (1980).
14. Sulston, J. E. & Horvitz, H. R. Abnormal cell lineages in mutants of the nematode *Caenorhabditis elegans*. *Dev. Biol.* **82**, 41–55 (1981).
15. Ambros, V. & Horvitz, H. R. Heterochronic mutants of the nematode *Caenorhabditis elegans*. *Science* **226**, 409–416 (1984).
16. Viswanathan, S. R., Daley, G. Q. & Gregory, R. I. Selective blockade of microRNA processing by Lin28. *Science* **320**, 97–100 (2008).
17. Zhu, H. et al. Lin28a transgenic mice manifest size and puberty phenotypes identified in human genetic association studies. *Nat. Genet.* **42**, 626–630 (2010).
18. Tsanov, K. M. et al. LIN28 phosphorylation by MAPK/ERK couples signalling to the post-transcriptional control of pluripotency. *Nat. Cell Biol.* **19**, 60–67 (2017).
19. Yermalovich, A. V. et al. Lin28 and let-7 regulate the timing of cessation of murine nephrogenesis. *Nat. Commun.* **10**, 168 (2019).
20. Osborne, J. K. et al. Lin28 paralogs regulate lung branching morphogenesis. *Cell Rep.* **36**, 109408–109408 (2021).
21. Kerepesi, C., Zhang, B., Lee, S.-G., Trapp, A. & Gladyshev, V. N. Epigenetic clocks reveal a rejuvenation event during embryogenesis followed by aging. *Sci. Adv.* **7**, eabg6082 (2021).
22. Shyh-Chang, N. et al. Lin28 enhances tissue repair by reprogramming cellular metabolism. *Cell* **155**, 778–792 (2013).
23. Polesskaya, A. et al. Lin-28 binds IGF-2 mRNA and participates in skeletal myogenesis by increasing translation efficiency. *Genes Dev.* **21**, 1125–1138 (2007).
24. West, J. A. et al. A role for Lin28 in primordial germ-cell development and germ-cell malignancy. *Nature* **460**, 909–913 (2009).
25. Keefe, A. C. et al. Muscle stem cells contribute to myofibres in sedentary adult mice. *Nat. Commun.* **6**, 7087 (2015).
26. Seale, P. et al. Pax7 is required for the specification of myogenic satellite cells. *Cell* **102**, 777–786 (2000).
27. Lepper, C., Partridge, T. A. & Fan, C. M. An absolute requirement for Pax7-positive satellite cells in acute injury-induced skeletal muscle regeneration. *Development* **138**, 3639–3646 (2011).
28. Der Vartanian, A. et al. PAX3 confers functional heterogeneity in skeletal muscle stem cell responses to environmental stress. *Cell Stem Cell* **24**, 958–973.e9 (2019).
29. de Morree, A. et al. Alternative polyadenylation of Pax3 controls muscle stem cell fate and muscle function. *Science* **366**, 734–738 (2019).
30. Schiaffino, S. & Reggiani, C. Fiber types in mammalian skeletal muscles. *Physiol. Rev.* **91**, 1447–1531 (2011).
31. Liu, L. et al. Isolation of skeletal muscle stem cells by fluorescence-activated cell sorting. *Nat. Protoc.* **10**, 1612–1624 (2015).
32. Horvath, S. DNA methylation age of human tissues and cell types. *Genome Biol.* **14**, 3156 (2013).
33. Horvath, S. & Raj, K. DNA methylation-based biomarkers and the epigenetic clock theory of ageing. *Nat. Rev. Genet.* **19**, 371–384 (2018).
34. Motohashi, N. & Asakura, A. Muscle satellite cell heterogeneity and self-renewal. *Front. Cell Dev. Biol.* **2**, 1 (2014).
35. Jaafar, R. et al. Phospholipase D regulates the size of skeletal muscle cells through the activation of mTOR signaling. *Cell Commun. Signal.* **11**, 55 (2013).
36. Bober, E., Franz, T., Arnold, H. H., Gruss, P. & Tremblay, P. Pax-3 is required for the development of limb muscles: a possible role for the migration of dermomyotomal muscle progenitor cells. *Development* **120**, 603–612 (1994).
37. Yusuf, F. et al. Inhibitors of CXCR4 affect the migration and fate of CXCR4+ progenitors in the developing limb of chick embryos. *Dev. Dyn.* **235**, 3007–3015 (2006).
38. Mercader, N. et al. Opposing RA and FGF signals control proximodistal vertebrate limb development through regulation of Meis genes. *Development* **127**, 3961–3970 (2000).
39. Capdevila, J., Tsukui, T., Esteban, C. R., Zappavigna, V. & Belmonte, J. C. I. Control of vertebrate limb outgrowth by the proximal factor Meis2 and distal antagonism of BMPs by Gremlin. *Mol. Cell* **4**, 839–849 (1999).
40. Heanue, T. A. et al. Synergistic regulation of vertebrate muscle development by Dach2, Eya2, and Six1, homologs of genes required for *Drosophila* eye formation. *Genes Dev.* **13**, 3231–3243 (1999).
41. Borsani, G. et al. EYA4, a novel vertebrate gene related to *Drosophila* eyes absent. *Hum. Mol. Genet.* **8**, 11–23 (1999).
42. Grifone, R. et al. Six1 and Six4 homeoproteins are required for Pax3 and Mrf expression during myogenesis in the mouse embryo. *Development* **132**, 2235–2249 (2005).
43. Jun-Hao, E. T., Gupta, R. R. & Shyh-Chang, N. Lin28 and let-7 in the metabolic physiology of aging. *Trends Endocrinol. Metab.* **27**, 132–141 (2016).
44. Relaix, F., Rocancourt, D., Mansouri, A. & Buckingham, M. A Pax3/Pax7-dependent population of skeletal muscle progenitor cells. *Nature* **435**, 948–953 (2005).
45. Tremblay, P. et al. A crucial role for Pax3 in the development of the hypaxial musculature and the long-range migration of muscle precursors. *Dev. Biol.* **203**, 49–61 (1998).
46. Ridgeway, A. G. & Skerjanc, I. S. Pax3 is essential for skeletal myogenesis and the expression of Six1 and Eya2. *J. Biol. Chem.* **276**, 19033–19039 (2001).
47. Grifone, R. et al. Eya1 and Eya2 proteins are required for hypaxial somitic myogenesis in the mouse embryo. *Dev. Biol.* **302**, 602–616 (2007).
48. Yang, D. H. & Moss, E. G. Temporally regulated expression of Lin-28 in diverse tissues of the developing mouse. *Gene Expr. Patterns* **3**, 719–726 (2003).
49. Yokoyama, S. et al. Dynamic gene expression of Lin-28 during embryonic development in mouse and chicken. *Gene Expr. Patterns* **8**, 155–160 (2008).
50. Buganim, Y. et al. Single-cell expression analyses during cellular reprogramming reveal an early stochastic and a late hierarchic phase. *Cell* **150**, 1209–1222 (2012).
51. Yu, J. et al. Induced pluripotent stem cell lines derived from human somatic cells. *Science* **318**, 1917–1920 (2007).
52. Goodell, M. A., Nguyen, H. & Shroyer, N. Somatic stem cell heterogeneity: diversity in the blood, skin and intestinal stem cell compartments. *Nat. Rev. Mol. Cell Biol.* **16**, 299–309 (2015).
53. Muller-Sieburg, C. E., Sieburg, H. B., Bernitz, J. M. & Cattarossi, G. Stem cell heterogeneity: implications for aging and regenerative medicine. *Blood* **119**, 3900–3907 (2012).
54. Boehm, M. & Slack, F. A developmental timing microRNA and its target regulate life span in *C. elegans*. *Science* **310**, 1954–1957 (2005).
55. de Magalhães, J. P. Programmatic features of aging originating in development: aging mechanisms beyond molecular damage? *FASEB J.* **26**, 4821–4826 (2012).
56. Darwin, C. *The Variation of Animals and Plants Under Domestication*, Vol. 1 (Cambridge University Press, 2010).
57. Poss, K. D. Advances in understanding tissue regenerative capacity and mechanisms in animals. *Nat. Rev. Genet.* **11**, 710–722 (2010).
58. Aalami, O. O. et al. Applications of a mouse model of calvarial healing: differences in regenerative abilities of juveniles and adults. *Plast. Reconstr. Surg.* **114**, 713–720 (2004).
59. Detwiler, S. R. Restitution of the brachial region of the cord following unilateral excision in the embryo. *J. Exp. Zool.* **104**, 53–68 (1947).
60. Holtzer, H. Reconstitution of the urodele spinal cord following unilateral ablation. Part I. Chronology of neuron regulation. *J. Exp. Zool.* **117**, 523–557 (1951).
61. Davis, B. M., Duffy, M. T. & Simpson, S. B. Jr Bulbospinal and intraspinal connections in normal and regenerated salamander spinal cord. *Exp. Neurol.* **103**, 41–51 (1989).
62. Wilson, A. A. et al. Lentiviral delivery of RNAi for in vivo lineage-specific modulation of gene expression in mouse lung macrophages. *Mol. Ther.* **21**, 825–833 (2013).
63. Tasic, B. et al. Site-specific integrase-mediated transgenesis in mice via pronuclear injection. *Proc. Natl. Acad. Sci. USA* **108**, 7902–7907 (2011).
64. Liu, T. M. et al. Ascorbate and iron are required for the specification and long-term self-renewal of human skeletal mesenchymal stromal cells. *Stem Cell Reports* **14**, 210–225 (2020).

ACKNOWLEDGEMENTS

This work was supported by the Strategic Priority Research Program of the CAS (XDA16010109), the National Key R&D Program of China (2019YFA0801700), the National Natural Science Foundation of China (91957202), and the Key Research Program of the CAS (KJZD-SW-L04). N.S.-C. is also a Howard Hughes Medical Institute (HHMI) International Scholar.

AUTHOR CONTRIBUTIONS

P.W. and X.L. designed and performed the experiments. P.W., X.L. and N.S.-C. wrote the manuscript. L. Guo helped with various experiments and mouse husbandry. J.-H.E.T., M.-W.J.C. and Y.-J.B.C. helped with HSKM and LTS cell experiments. L.L. helped with cryosection and immunofluorescence experiments. S.M. helped with

Western blot experiments. W.C. helped with qRT-PCR experiments. W.M., N.A., Y.L. and L.J. helped with bioinformatics analysis. Z.Y., Y.C., K.L., L. Guang, Y.W., H.Z., R.R.W. and C.L. provided technical assistance. L.Z. and S.L. helped with mouse sampling. B.T.T., K.Y. and N.S.-C. designed and supervised the overall project.

COMPETING INTERESTS

The authors declare no competing interests.

ADDITIONAL INFORMATION

Supplementary information The online version contains supplementary material available at https://doi.org/10.1038/s41422-023-00818-y.

Correspondence and requests for materials should be addressed to Ng Shyh-Chang.